SIAM J. APPL. MATH.
Vol. 65, No. 2, pp. 392–425

SYNCHRONY IN A POPULATION OF HYSTERESIS-BASED GENETIC OSCILLATORS*

ALEXEY KUZNETSOV†, MADS KÆRN‡, AND NANCY KOPELL†

Abstract. Oscillatory behavior has been found in different specialized genetic networks. Previous work has demonstrated nonsynchronous, erratic single-cell oscillations in a genetic network composed of nonspecialized regulatory components and based entirely on negative feedback. Here, we present the construction of a more robust, hysteresis-based genetic relaxation oscillator and provide a theoretical analysis of the conditions necessary for single-cell and population synchronized oscillations. The oscillator is constructed by coupling two subsystems that have previously been implemented experimentally. The first subsystem is the toggle switch, which consists of two mutually repressive genes and can display robust switching between bistable expression states and hysteresis. The second subsystem is an intercell communication system involved in quorum-sensing. This subsystem drives the toggle switch through a hysteresis loop in single cells and acts as a coupling between individual cellular oscillators in a cell population. We demonstrate the possibility of both population synchronization and suppression of oscillations (cluster formation), depending on diffusion strength and other parameters of the system. We also propose the optimal choice of the parameters and small variations in the architecture of the gene regulatory network that substantially expand the oscillatory region and improve the likelihood of observing oscillations experimentally.

Key words. coupled oscillators, relaxation oscillations, stability, intercell communication, gene networks

AMS subject classifications. 34C15, 34C26, 92D10

DOI. 10.1137/S0036139903436029

1. Introduction.

The variation in gene expression in response to internal or external signals is one of the most important means of cellular regulation. The rate at which a gene is transcribed into messenger RNA and subsequently translated into protein is influenced by many factors but is primarily controlled by how well the RNA polymerase complex can bind to and initiate transcription from a regulatory region of the DNA called the promoter. Signals that modulate transcription are often mediated through transcription factor proteins that bind to target sites within or near the promoter where they increase (activation) or decrease (repression) the probability of RNA polymerase complex binding and/or initiation of transcription. The manipulation of DNA sequence to create novel promoters containing customized transcription factor target sites and to mix and match such promoters with genes that encode the corresponding transcription factor proteins has allowed the construction of artificial gene regulatory networks with customizable functionality [1, 2, 3, 4, 5]. Such networks can be used to achieve complex and multifaceted control of cellular function and have promising scientific, medicinal, and biotechnological applications [6, 7, 8].

*Received by the editors October 8, 2003; accepted for publication (in revised form) May 12, 2004; published electronically December 16, 2004.
http://www.siam.org/journals/siap/65-2/43602.html

†Center for BioDynamics and Mathematical Department, Boston University, 111 Cummington St., Boston, MA 02215 (alexey@bu.edu, nk@bu.edu). The work of the first author was partially supported by NSF grant DMS-0109427. The work of the third author was partially supported by NSF grant DMS-0211505.

‡Center for BioDynamics and Biomedical Engineering Department, Boston University, 44 Cummington St., Boston, MA 02215 (mkaern@bu.edu). The work of this author was partially supported by NSF Bio-QuBIC Program grant EIA-0130331 and The Defense Advanced Research Projects Agency grant F30602-01-2-0579.

Mathematical modeling and analysis is becoming increasingly important as a tool to organize and to interpret vast amounts of experimental data and as a predictive tool in the construction of artificial gene networks [1, 2, 9]. The first step in the construction of an artificial gene network is to investigate if the proposed network architecture supports the desired functionality. In this paper, we use mathematical techniques to model and analyze an artificial gene network that is currently being implemented experimentally in the bacterium *Escherichia coli* [10]. The network is intended to regulate a population synchronous periodic oscillation in the levels of cellular protein in a constant density, well-stirred bio-reactor. The goals of the mathematical analysis are (1) to investigate if the network architecture supports single-cell and population synchronous oscillations, (2) to identify the parameter values and the experimental conditions where this behavior is supported, and (3) to suggest modifications to the network that optimize the robustness of single-cell and population oscillations.

The oscillator is to be constructed by combining two engineered gene networks that have previously been implemented experimentally in *E. coli*: the toggle switch [1] and an intercell communication system [11, 12, 13]. The engineered gene networks are carried on multicopy, self-replicating plasmids that interfere minimally with the host cell. As a result, the dynamics of the engineered networks may be considered independently of the dynamics of the cell's natural regulatory circuitry. The toggle switch is composed of two transcription factor proteins: the lac repressor, encoded by the gene *lacI*, and a temperature-sensitive variant of the λ *cI* repressor, encoded by the gene *cI857*. The synthesis of the two repressor proteins is regulated in such a way that expression of the *cI857* and *lacI* genes are mutually exclusive: The promoter P_{trc} that controls the expression of *cI857* is attenuated by the lac repressor while the promoter P_{L*} that controls the expression of *lacI* is attenuated by the λ repressor. Thus, a cell can be either in a state where λ repressor is abundant and lac repressor scarce (the *cI* on state) or in a state where lac repressor is abundant and λ repressor scarce (the *lacI* on state).

It has been demonstrated experimentally [1] that the state of cells harboring the toggle switch network can be changed permanently by transient inactivation of the dominant repressor protein. The λ repressor is inactivated at elevated temperature and the state can be changed from the *cI* ON to the *lacI* ON state by a transient increase in temperature. Conversely, the transition from the *lacI* ON to *cI* ON state ensues when the lac repressor protein is inactivated by the addition of sufficient amounts of the chemical isopropyl-β-D-thiogalactopyranoside (IPTG). At subcritical levels of IPTG, both states exist and are stable. Variation in IPTG has demonstrated hysteresis of these two steady states [1]. We exploit the presence of hysteresis in the toggle switch to construct an oscillator network by linking the toggle switch to a second network that autonomously drives cells through the hysteresis loop (Figure 1.1(A)).

The gene network intended to drive the oscillation involves components of the quorum-sensing system from *Vibrio fischeri* [14]. Quorum-sensing enables cells to sense population density through a transcription factor protein LuxR, which acts as a transcriptional activator of genes expressed from the P_{lux} promoter when a small organic molecular, the autoinducer (AI), binds to it. The AI is synthesized by the protein encoded by the gene *luxI*, and the AI can diffuse across the cell membrane causing the extracellular concentration of AI, as well as the AI concentration in individual cells, to depend on the density of AI-producing cells. These properties of the quorum-sensing system has been exploited experimentally to construct biosensors (see, e.g., [15, 16, 17]) to transfer information from one cell to another [11] and can,

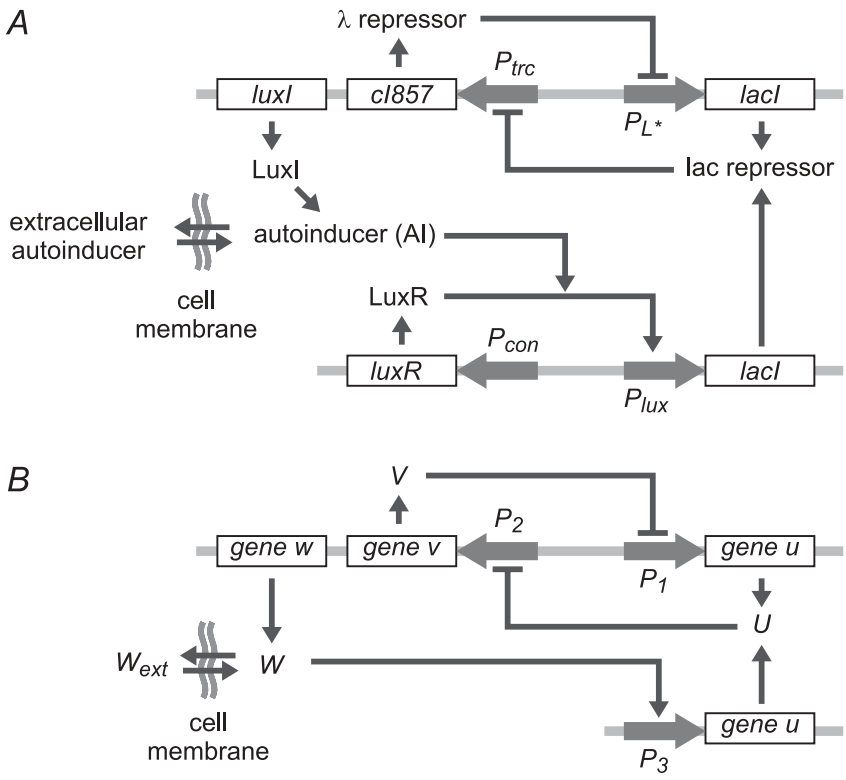

FIG. 1.1. *Schematic diagrams of the genetic oscillator network in isolated cells.* (A) *Full network composed of the toggle switch genes* cI857 *and* lacI *and their respective promoters* P_{trc} *(lac repressed) and* P_{L*} *(*λ *repressed) and the quorum-sensing genes* luxI *and* luxR*. Autoinducer* (AI) *is synthesized by the LuxI protein and activates expression of* lacI *from the* P_{lux} *promoter through binding to the LuxR transcription factor.* (B) *Minimal model. It is assumed that the activation of expression of the repressor gene u (*lacI*) occurs in a single step binding of W (AI) to the promoter* P_3 *(*P_{lux}*).*

in theory, be used to achieve synchronization across a cell population [18]. It was recently shown experimentally [10] that a variant of the network in Figure 1.1 lacking the *luxI* gene can respond to AI and be driven through a saddle-node bifurcation by increasing AI concentration.

This paper is organized as follows. In section 2, we discuss the structure of the genetic network and derive the equations that govern the dynamics of a minimal description of the network. In section 3, we investigate the dynamics of isolated cells and establish the condition for the organization of single-cell oscillations. In section 5, we consider the dynamics of an ensemble of cells and demonstrate the possibility of both population synchronization and suppression of oscillations, depending on diffusion strength and other parameters of the system. In section 4, we investigate the effect on the ability of isolated cells to oscillate when molecular details left out of the minimal model are taken into consideration. In particular, production of the autoinducer in two steps, rather than just one as assumed in the minimal model, improves the likelihood of observing oscillations experimentally. We also show that oscillatory behavior can be made much more robust by adding an additional connectivity to the network.

2. Minimal model. The molecular details of the genetic oscillator network that we wish to construct is illustrated schematically in Figure 1.1(A). It is a slight variant of a network constructed by Kobayashi et al. [10], where *luxI* is inserted downstream of *cI857* rather than downstream of *luxR*. The expression of the *cI857* is controlled by the promoter P_{trc}, and the expression of the *lacI* gene is controlled by the P_{L*} promoter. As a result, the AI is synthesized when the cell is in the *cI* ON/*lacI* OFF state. The AI binds to the LuxR protein, whose gene is expressed at a constant rate from the P_{con} promoter, and the LuxR-AI complex increases the rate of expression of the *lacI* gene by activation of the P_{lux} promoter. Hence, when cells are in the *lacI* OFF state, the AI will gradually accumulate and activate the production of λ repressor protein. The λ repressor eventually shuts down expression of *cI* and *luxI* from the P_{trc} promoter, causing a transition from the *cI* ON to the *lacI* ON state and a down-regulation of AI production. To complete the cycle, it is required that a cell returns to the *cI* ON state once AI production ceases in the *lacI* ON state. Therefore, oscillations require that the toggle switch component of the network is bistable at intermediate levels of AI and monostable when the level of AI is either high (*lacI* ON) or low (*cI* ON).

To ease the mathematical analysis, we initially employ a simplified model of the full system, illustrated in Figure 1.1(B). In this model, the promoters are renamed P_1 (P_{L*}), P_2 (P_{trc}), and P_3 (P_{lux}) and the transcription factors renamed U (lac repressor), V (λ repressor), and W (the LuxR-AI activator). The difference between the full (Figure 1.1(A)) and the simplified system (Figure 1.1(B)) lies in the regulation of the P_3 promoter. We assume for simplicity that the activator of P_3 is encoded by a single gene w rather than being the complex between LuxR and the AI. This assumption ignores a potential time delay introduced by the two-step synthesis of the LuxR-AI complex (i.e., LuxI $\rightarrow$ AI $\rightarrow$ LuxR-AI) and the titration and saturation of free LuxR by the AI. The effects of these assumptions on oscillations in single cells are investigated further in section 4.

2.1. Regulation of gene expression. The simplest model of gene expression involves only two steps: the transcription of a gene into mRNA and the translation of the mRNA into protein [19]. Consider the expression of a gene x that encodes the protein X and is regulated by the promoter P. When each cell harbors n_A active promoters from which the mRNA of gene x is transcribed at an average rate k, the approximation of the rate of mRNA change gives us the following differential equation:

$$\frac{dn_m}{dt} = n_A k - d_m n_m, \tag{2.1}$$

where d_m is the effective first-order rate constant associated with degradation of the mRNA within cells. This equation is, of course, only an approximation since it assumes that the number of mRNA molecules is continuous rather than discrete and since many additional steps are involved in both transcription and degradation of mRNA [21]. Messenger RNA molecules are usually degraded rapidly compared to other cellular processes, and it is often assumed that the concentration of mRNA rapidly reaches a pseudo-steady state where $n_m = n_A k/d_m$ such that dn_m/dt is zero. In some cases, the delay introduced by mRNA synthesis is important for oscillatory dynamics [2]. However, mRNA half-lives are difficult to manipulate experimentally, which makes it difficult to exploit these control parameters in vivo.

The mRNA is translated into a protein by ribosomes, and it is assumed that each x mRNA molecule gives rise to $b_x = k_{tl,x}/d_m$ copies of the protein X, where

$k_{tl,x}$ is the averaged translation rate. The parameter b_x is referred to as the burst parameter of the protein and depends on the efficiency of translation and the mRNA half-life [19]. The value of the translational efficiency depends, among several factors, on the nucleotide sequence of the ribosome binding sites (RBS) located within the upstream, noncoding part of the mRNA. The RBS is encoded by the DNA sequence immediately upstream of the start codon of the gene and is an independent regulatory element that can be manipulated experimentally. The sequence of the DNA encoding the RBS is one of the principal tools by which the parameters of an engineered gene network can be adjusted (see, e.g., [1]).

The equation that governs the evolution of the number of proteins, n_X, produced from n_m mRNA molecules is in the continuous approximation given by

$$\frac{dn_X}{dt} = k_{tl,x} n_m - k_X n_X, \tag{2.2}$$

where $k_{tl,x}$ is the averaged translation rate, introduced above and k_X is the effective first-order rate constant associated with the degradation of the protein within cells. When a pseudo-steady state approximation is invoked for mRNA ($n_m = n_A k/d_m$), it is obtained that $k_{tl,x} n_m = k_{tl,x} n_A k/d_m = b_x n_A k$. The equation for the number of proteins takes the form

$$\frac{dn_X}{dt} = b_x n_A k - k_X n_X. \tag{2.3}$$

The rate of protein decay, k_X, is a second experimental control parameter that can be altered by augmenting, or tagging, the protein with additional amino acids, which makes the protein a target of proteases that break down the protein into amino acids [2].

It is convenient to convert the equation for the evolution of the total number of proteins per cell into an equation for the evolution of cellular protein concentration, $[X](t) = n_X(t)/v(t)$, where $v(t)$ is the cell volume. Cells divide at regular time intervals T, and the cell volume is assumed to increase exponentially in accordance with the growth law $v(t) = v_0 \exp(k_g t)$, where v_0 is the cell volume immediately after division and $k_g = \ln(2)/T$. Cell division occurs when $v(t = T) = 2v_0$. The evolution equation for protein concentration is then obtained as

$$\frac{d[X]}{dt} = \frac{1}{v(t)} \left(\frac{dn_X}{dt} - [X] \frac{dv(t)}{dt} \right) = b_x k [A](t) - (k_X + k_g)[X], \tag{2.4}$$

where $[A](t)$ is the concentration of active promoters, $[A](t) = n_A(t)/v(t)$. It is noted that an exponential increase in cell volume is only an approximation of the quite complicated process of cell growth and division.

The concentration of active promoters, $[A](t)$, depends on the concentration of transcription factors that are bound to the promoter region at a given time. Consider the formation of a complex PE between the promoter, P, and a transcriptional effector E of that promoter through the cooperative binding of β effector molecules to the unoccupied promoter. This scheme can be represented by the reversible chemical reaction of the Hill type with the equilibrium constant K:

$$\beta E + P \leftrightarrows PE, \quad K = \frac{[PE]}{[E]^\beta [P]}, \tag{2.5}$$

where $[P]$, $[PE]$, and $[E]$ are the concentrations of unoccupied promoters, occupied promoters, and effector molecules, respectively. The parameter β is the Hill coefficient associated with the binding of the effector to the promoter.

The total concentration of promoters is proportional to the concentration $[P_{tot}]$ of the plasmid that carries the promoter. Plasmids are self-replicating, and the total number of plasmids (and, hence, of promoters) change as a cell progresses through the division cycle. The control of the plasmid copy number is quite elaborate [20] and must be balanced with the cell's growth and division. As a first approximation, it is assumed that the number of plasmids per cell scales proportionally with the cell volume such that the plasmid concentration remains fairly constant throughout the cell division cycle, i.e., that $[P_{tot}] = [P](t) + [PE](t)$ is constant. Combined with the equilibrium relation in (2.5), the conservation of plasmid concentration can be used to derive the concentration of active promoters $[A]$ used in (2.4). The effector can be either a transcriptional repressor or a transcriptional activator. In the case when the effector is the repressor, the unoccupied promoters are supposed to be active, and $[A]^R \equiv [P]$, where the superscript R stands for the repression case. Deriving concentration of the repressed promoters, $[PE]$, from (2.5) as a function of $[P]$, we have $[P_{tot}] = [P] + K[E]^\beta[P]$, or, taking into account the equivalence of $[P]$ and $[A]^R$, $[P_{tot}] = [A]^R + K[E]^\beta[A]^R$. Then, in the case of transcriptional repression, the concentration of active promoters is given by

$$[A]^R = \frac{[P_{tot}]}{1 + K[E]^\beta}. \tag{2.6}$$

In the case when the effector is the activator, the unoccupied promoters are assumed to be passive, and $[A]^A \equiv [PE]$, where the superscript A stands for the activation case. We derive concentration of unoccupied promoters from (2.5) as $[P] = [A]^A/K[E]^\beta$, then $[P_{tot}] = [A]^A/K[E]^\beta + [A]^A$. From this equation, the concentrations of active promoters is given by

$$[A]^A = \frac{[P_{tot}]K[E]^\beta}{1 + K[E]^\beta}. \tag{2.7}$$

Introducing the exponent a, we can write down the common formula for these two cases:

$$[A] = \frac{[P_{tot}]\left\{K[E]^\beta\right\}^a}{1 + K[E]^\beta}, \tag{2.8}$$

where the case of repression (R) corresponds to $a = 0$ and the case of activation (A) corresponds to $a = 1$.

Equation (2.4) can be generalized for the case of multiple promoters, controlling the production of the same protein. Suppose we have several protein effectors E_j, each of which influences production of the protein X, binding the corresponding promoter P_j ($j = 1, \dots, M$). By summation of the contribution from each promoter P_j in the network, the evolution of the protein concentration $[X]$ can be written as

$$\frac{d[X]}{dt} = \sum_{j=1}^{M} \frac{b_{jx}k_j[P_{tot,j}][K_j[E_j](t)^{\beta_j}]^{a_j}}{1 + K_j[E_j](t)^{\beta_j}} - (k_X + k_g)[X]. \tag{2.9}$$

We also need to take into account that X may be able to penetrate the cell membrane by passive or active transport. An additional term for (2.9), which corresponds

to the passive transport, is $D_X([X] - [X_{ext}])$. Here, $[X_{ext}]$ is the extracellular concentration of X and D_X is an effective diffusion coefficient. The parameter D_X, in its simplest form, is defined by $D_X = S(t)p_X/v(t)$, where $S(t)$ is the cell surface area and p_X is the membrane permeability of X [22]. While D_X depends slightly on the stage of the cell division cycle, we will assume for simplicity that D_X is a constant. The resulting equation for a protein, which is synthesized from multiple promoters and can penetrate the cell membrane, is given by

$$\frac{d[X]}{dt} = \sum_{j=1}^{M} \frac{b_{jx}k_j[P_{tot,j}][K_j[E_j](t)^{\beta_j}]^{a_j}}{1 + K_j[E_j](t)^{\beta_j}} - (k_X + k_g)[X] - D_X([X] - [X_{ext}]). \tag{2.10}$$

Most proteins within the cell are unable to penetrate the cell membrane, and the diffusive term is in the present case only relevant for the AI.

2.2. The genetic oscillator model. The network diagram in Figure 1.1(B) can be converted into a system of evolution equations by using (2.10) for each of the three proteins U, V, and W synthesized from the three promoters. We use $[U]_i$, $[V]_i$, and $[W]_i$ to denote the concentrations of U, V, and W in cell i and $[W_{ext}]$ to denote the extracellular concentration of the AI:

$$\begin{aligned}
\frac{d[U]_i}{dt} &= \frac{b_{1u}k_1[P_{tot,1}]}{1 + K_1[V]_i^{\beta}} + \frac{b_{3u}k_3[P_{tot,3}]K_3[W]_i^{\eta}}{1 + K_3[W]_i^{\eta}} - (k_U + k_g)[U]_i, \\
\frac{d[V]_i}{dt} &= \frac{b_{2v}k_2[P_{tot,2}]}{1 + K_2[U]_i^{\gamma}} - (k_V + k_g)[V]_i, \\
\frac{d[W]_i}{dt} &= \frac{b_{2w}k_2[P_{tot,2}]}{1 + K_2[U]_i^{\gamma}} - (k_W + k_g)[W]_i - D_W([W]_i - [W_{ext}]),
\end{aligned} \tag{2.11}$$

where β, γ, and η denote the Hill coefficients of the P_1, P_2, and P_3 promoter, respectively.

Since the AI is able to penetrate the cell membrane, it is necessary to consider how the production of AI in an ensemble of N cells changes the extracellular AI concentration. The flux ϕ_i (in number/time unit) of W across the membrane of an individual cell is $\phi_i = S(t)p_W([W]_i - [W_{ext}])$ [22], and the evolution of the extracellular autoinducer concentration is given by

$$\frac{d[W_{ext}]}{dt} = \frac{v_c D_W}{v_{ext}} \frac{1}{N} \sum_{i=1}^{N} ([W]_i - [W_{ext}]) - k_0[W_{ext}], \tag{2.12}$$

where v_{ext} is the volume of the extracellular space, v_c is the total volume of N cells, and k_0 is the effective first-order constant of removal of AI from the extracellular medium. We assume that the experiments are carried out in a continuously stirred, constant volume flow reactor where the extracellular medium is homogeneous and the number of cells is kept constant by continuous dilution of the cell culture by a steady inflow of fresh growth medium and outflow of extracellular medium and cells. It is the rate of this dilution that determines the value of the parameter k_0.

To reduce the number of parameters in the system, we assume that U and V have identical half-lives, $k_d = k_U = k_V$. This assumption is based on the fact that the protein decay rate can be controlled in experiments. The identical half-lives are determined by identical protease tags added to these proteins. However, this assumption is not a constraint for design of the network but just a simplification for

our analysis. To normalize the equations, we introduce the following dimensionless variables:

$$u_i = \sqrt[\gamma]{K_2}[U]_i, \quad v_i = \sqrt[\beta]{K_1}[V]_i, \quad w_i = \sqrt[\eta]{K_3}[W]_i,$$
$$w_e = \sqrt[\eta]{K_3}[W_{ext}], \quad \tau = (k_d + k_g)t. \tag{2.13}$$

With these assumptions, the system is governed by the dimensionless system:

$$\begin{aligned}
\frac{du_i}{d\tau} &= \alpha_1 f(v_i) + \alpha_3 h(w_i) - u_i,\\
\frac{dv_i}{d\tau} &= \alpha_2 g(u_i) - v_i,\\
\frac{dw_i}{d\tau} &= \bar{\alpha}_2 g(u_i) - \delta w_i - D(w_i - w_e),\\
\frac{dw_e}{d\tau} &= \frac{D_e}{N}\sum_{i=1}^{N}(w_i - w_e) - \delta_e w_e,
\end{aligned} \tag{2.14}$$

where the functions are defined by

$$f(v) = \frac{1}{1+v^\beta}, \quad g(u) = \frac{1}{1+u^\gamma}, \quad h(w) = \frac{w^\eta}{1+w^\eta}, \tag{2.15}$$

and the dimensionless parameters are defined by

$$\begin{aligned}
\alpha_1 &= \frac{\sqrt[\gamma]{K_2} b_{1u} k_1 [P_{tot,1}]}{k_d + k_g}, \quad \alpha_2 = \frac{\sqrt[\beta]{K_1} b_{2v} k_2 [P_{tot,2}]}{k_d + k_g},\\
\bar{\alpha}_2 &= \frac{\sqrt[\eta]{K_3} b_{2w} k_2 [P_{tot,2}]}{k_d + k_g}, \quad \alpha_3 = \frac{\sqrt[\gamma]{K_2} b_{3u} k_3 [P_{tot,3}]}{k_d + k_g},\\
\delta &= \frac{k_W + k_g}{k_d + k_g}, \quad \delta_e = \frac{k_0}{k_d + k_g}, \quad D = \frac{D_W}{(k_d + k_g)}, \quad D_e = \frac{v_c D_W}{v_{ext}(k_d + k_g)}.
\end{aligned} \tag{2.16}$$

3. Isolated element. We first establish the conditions for oscillations in isolated cells. Cells can be considered as isolated elements in the limit $D_e \ll \delta_e$, corresponding to a vanishing cell density, where the contribution from cellular autoinducer production to the extracellular autoinducer concentration is vanishing and $w_e \to 0$. The evolution of protein content in an isolated cell is thus determined by

$$\begin{aligned}
&\frac{du}{d\tau} = \alpha_1 f(v) + \alpha_3 h(w) - u, \quad \frac{dv}{d\tau} = \alpha_2 g(u) - v,\\
&\frac{dw}{d\tau} = \bar{\alpha}_2 g(u) - (D+\delta)w = \varepsilon\left(\alpha_4 g(u) - w\right),
\end{aligned} \tag{3.1}$$

where $\varepsilon = D + \delta = (D_W + k_g)/(k_d + D_W)$ and $\alpha_4 = \bar{\alpha}_2(k_d + D_W)/(D_W + k_g)$. We suppose also that $\bar{\alpha}_2$ is of the same order as $(D+\delta)$, i.e., $\alpha_4 = O(1)$ because otherwise dynamics becomes trivial (the only stationary state).

When the parameter ε is small ($\varepsilon \ll 1$), the evolution of the system splits into two well-separated time-scales. In the fast time-scale, changes of the coordinates per unit of time τ are of order 1. Here, we can assume w to be stationary, since $dw/d\tau \sim \varepsilon \ll 1$. The fast motion ceases in the vicinity of the curve, where $du/d\tau = 0$ and $dv/d\tau = 0$, which is called the manifold of slow motion. On the manifold, changes of the coordinates per unit of time τ are of order ε, and we can introduce the slow time $\tau_1 = \varepsilon\tau$, where the changes are of order 1.

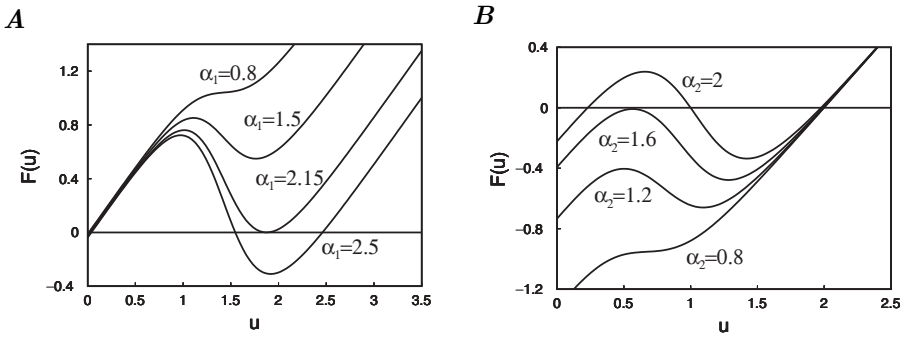

FIG. 3.1. *Geometrical investigation of equilibrium states in the fast subsystem with* $\alpha_w = 0$. *Equilibrium states are located where* $F(u) = 0$. (A) *Increasing the value of* α_1 *causes a transition from one to three equilibrium states, with a new equilibrium with high* u *being created through a saddle-node bifurcation. Parameter values are* $\alpha_2 = 4$, $\beta = \gamma = 3$. (B) *Creation of an equilibrium state with low* u *through a saddle-node bifurcation by an increase in* α_2. *Parameter values are* $\alpha_1 = 2$, $\beta = \gamma = 3$.

3.1. The fast subsystem. The first step in our analysis is to establish the conditions where the fast subsystem can be driven through a bistability region by varying the autoinducer concentration. Two conditions must be satisfied by the fast subsystem. (1) Two saddle-node bifurcations that define a region of bistability must exist and (2) the bifurcations must occur as the autoinducer concentration is varied. To establish the analytical conditions, we look for equilibria on the fast time-scale for $\varepsilon \to 0$, where the full system reduces to the toggle switch equations [1] augmented with a constant production term α_w arising from a constant concentration of autoinducer:

$$\begin{aligned} \frac{du}{d\tau} &= \alpha_1 f(v) + \alpha_w - u = P(u,v), \\ \frac{dv}{d\tau} &= \alpha_2 g(u) - v = Q(u,v), \end{aligned} \tag{3.2}$$

where $\alpha_w = \alpha_3 h(w)$. These equations correspond to those used by Kobayashi et al. to guide the construction of a toggle-based AI biosensor [10]. By Bendixson's criterion [23], the system in (3.2) has no closed orbit since the divergence of the vector field $P_u' + Q_v' = -2$ does not change sign.

3.1.1. Absence of autoinducer. In the absence of the autoinducer ($\alpha_w = 0$), the equilibrium states (u_0, v_0) of the system in (3.2) can be found by setting $v = \alpha_2 g(u)$ as the zeros of the function $F(u)$ given by

$$F(u) = u - \alpha_1 f\left(\alpha_2 g(u)\right) = u - \frac{\alpha_1 (1+u^\gamma)^\beta}{\alpha_2^\beta + (1+u^\gamma)^\beta}. \tag{3.3}$$

Since $F(u) \to -\alpha_1/(\alpha_2^\beta + 1) < 0$ for $u \to 0$ and $F(u) \to u - \alpha_1 > 0$ for $u \to \infty$, the existence of at least one steady state is guaranteed.

A necessary, but not sufficient, condition for the existence of multiple equilibrium states is that $F(u)$ be an N-shaped function such that there exist local extrema (where $F'(u) = 0$). Figure 3.1 illustrates the transition from monostability when α_1 is varied for $\alpha_2 = 4$, $\beta = \gamma = 3$. At very low values of α_1, the function $F(u)$ is monotonically increasing and there exists a single equilibrium state where u_0 is low and v_0 is high.

When α_1 increases, a local maximum and a local minimum emerge, but there is still only a single equilibrium state. As α_1 increases further, the local minimum of $F(u)$ is shifted downward, and it coincides with $F(u) = 0$ when α_1 reaches a critical value α_1^c (at approximately $\alpha_1 = 2.14925$ in Figure 3.1). This critical point corresponds to a saddle-node bifurcation where the two conditions $F(u) = 0$ and $F'(u) = 0$ are simultaneously fulfilled and a new equilibrium state is created. For α_1 higher than the critical value, the function $F(u)$ has three zeros corresponding to three equilibrium states. Two of these states are destroyed when α_1 is very high (greater than approximately 22.9767 for $\alpha_2 = 4$, $\beta = \gamma = 3$) where the local maximum is shifted to negative values of $F(u)$ (not shown). The system is again monostable, this time with an equilibrium state where u_0 is high and v_0 is low. As illustrated in Figure 3.1(B), a similar bifurcation scenario is observed when α_2 is varied.

The characteristic polynomial that determines stability of the equilibrium states of the fast subsystem is given by

$$\begin{aligned} \lambda^2 + 2\lambda + F'(r) &= 0, \\ F'(r) &= 1 - \alpha_1\alpha_2 f_v'(v_0(r))g_u'(r), \end{aligned} \tag{3.4}$$

where we have introduced the parameter r to represent the equilibrium state (u_0, v_0). This parameter is obtained from (3.1) by setting $du/d\tau = 0$ and $dv/d\tau = 0$:

$$r = u_0, \quad v_0 = \alpha_2 g(r). \tag{3.5}$$

It can be shown that when a single equilibrium state exists, it is always stable (monostability), and when three equilibrium states exist, one of them is unstable and the remaining two are stable (bistability).

As described above, the transition from monostability to bistability occurs through saddle-node bifurcations. Their location can be predicted from (3.4) by finding solutions where $\lambda = 0$, i.e., from $F'(r) = 0$. This equation can be written in a parametric form (Appendix A) to obtain sets of critical parameter values $(\alpha_1^c(r), \alpha_2^c(r))$ that determine the location of the saddle-node bifurcations in the α_1, α_2 phase plane:

$$\begin{aligned} \alpha_1^c(r) &= \tfrac{\beta\gamma r^{\gamma+1}}{1+r^\gamma} \Big/ \left(\tfrac{\beta\gamma r^\gamma}{1+r^\gamma} - 1\right), \\ \alpha_2^c(r) &= (1+r^\gamma)\left(\tfrac{\beta\gamma r^\gamma}{1+r^\gamma} \Big/ \left(\tfrac{\beta\gamma r^\gamma}{1+r^\gamma} - 1\right) - 1\right)^{1/\beta}. \end{aligned} \tag{3.6}$$

In these equations, r is in the range $(r_l : \infty)$ with r_l defined by $r_l^\gamma = (\beta\gamma - 1)^{-1}$ (implying that $\beta\gamma > 1$ since r_l must be positive). Note that $\alpha_1^c(r) < 0$ when $r < r_l$, which violates the condition that all the parameters must be positive reals.

3.1.2. Presence of autoinducer. In the presence of autoinducer ($\alpha_w > 0$), the equilibrium states are obtained as the solution of $F(u) = \alpha_w$ rather than $F(u) = 0$. In order to use variation in α_w to drive the fast subsystem through a bistability region, it is essential that an increase (or decrease) in α_w causes the fast subsystem to pass through the two saddle-node bifurcations. Therefore, the system must be monostable when α_w is lower than a critical value $\alpha_w^+ > 0$, having the only equilibrium with low u (denoted r^-), monostable when α_w is greater than the second critical value $\alpha_w^- > \alpha_w^+$, having the only equilibrium with high u (denoted r^+), and bistable when $\alpha_w^- > \alpha_w > \alpha_w^+$. This scenario is depicted in Figure 3.2(A), where one, two, or three equilibrium states arises as α_w is varied. The critical values in α_w, where the fast

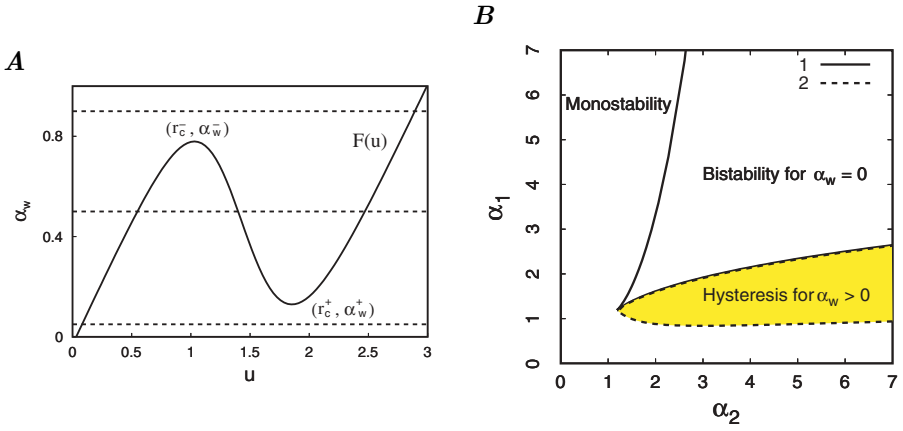

FIG. 3.2. (A) *Changes in the number of equilibrium states by variation in* α_w. *At* $\alpha_w = 0.05$ *there is a single equilibrium state at low* u. *There are three equilibrium states at* $\alpha_w = 0.5$ *and a single equilibrium state for* $\alpha_w = 0.9$. *The points labeled* (r_c^-, α_w^-) *and* (r_c^+, α_w^+) *correspond to the values of* α_w *at the saddle-node bifurcations. Parameter values are* $\alpha_1 = 2, \alpha_2 = 4$, $\beta = \gamma = 3$. (B) *Different regions of the* α_1, α_2 *phase plane showing different behavior for* $\beta = \gamma = 3$. *The solid curve encloses a region where the system is bistable in the absence of autoinducer. The solid and the dashed curve enclose a region where bistability can occur in the presence of autoinducer, i.e., a hysteresis loop for* $\alpha_w > 0$.

subsystem has two equilibrium states (a stable node and a saddle-node), satisfy the conditions

$$\alpha_w^- = F(r_c^-), \quad \alpha_w^+ = F(r_c^+), \quad F'(r_c^\pm) = 0, \tag{3.7}$$

where $r_c^\pm$ are the values of u corresponding to the extrema of $F(u)$.

To achieve hysteresis when α_w is varied, $F(u)$ must have two extrema and they must be located in the positive quadrant, i.e., $F(r_c^\pm) > 0$. The section of parameter plane where the fast subsystem satisfies the required conditions are thus bounded by two curves: one where bistability ceases to exist, corresponding to the merger of extrema of $F(u)$, and one where the minimum of $F(u)$ crosses into negative values. As derived in Appendix B, the merging extrema of the function $F(u)$ defines a curve $(\alpha_1^m(r), \alpha_2^m(r))$ in the α_1, α_2 phase plane given by

$$\alpha_1^m(r) = \frac{(1+r^\gamma)[1+R_1(r)]^2}{\gamma\beta R_1(r) r^{\gamma-1}}, \quad \alpha_2^m(r) = (1+r^\gamma) R_1(r)^{1/\beta}, \tag{3.8}$$

where

$$R_1(r) = -\frac{(\gamma-1) - r^\gamma(1+\beta\gamma)}{(\gamma-1) - r^\gamma(1-\beta\gamma)}. \tag{3.9}$$

The curve $(\alpha_1^m(r), \alpha_2^m(r))$ is in addition subject to the condition that the system is monostable in the absence of autoinducer. In other words, $F(u) = \alpha_w$ must have a single solution for $\alpha_w = 0$ and the saddle-node bifurcations must therefore occur at values of $\alpha_w = F(u) > 0$. The boundary of this condition coincides with that of emergence of bistability in the unperturbed toggle switch, which is determined by the curves of saddle-node bifurcations in (3.6). Figure 3.2(B) illustrates the regions of different dynamics in the α_1, α_2 parameter space. The solid curve is obtained

from (3.6), and the dashed curve shows the merging of extrema (3.8). The area enclosed by the solid curves corresponds to the region in parameter space where the fast subsystem shows bistability in the absence of autoinducer, and the shaded area corresponds to the region of parameter space where there exists a bistable region for $0 < \alpha_w^+ < \alpha_w < \alpha_w^-$, where α_w^+ and α_w^-, as previously defined in this section, are the critical values of autoinducer at the saddle-node bifurcations (see Figure 3.2(A)).

3.2. The slow subsystem. Given sufficient time-scale separation, the fast subsystem reaches a point on the manifold of slow motion, where the dynamics is governed by

$$\frac{dw}{d\tau} = \varepsilon(\alpha_4 g(u) - w). \tag{3.10}$$

Here u satisfies the condition $F(u) = \alpha_3 h(w)$ obtained from (3.2). When the parameters of the fast subsystem are such that there exist two extrema of $F(u)$ at $u = r_c^-$ (the local maximum) and $u = r_c^+$ (the local minimum), the slow subsystem can drive the fast subsystem through a bistability region if $\alpha_w = \alpha_3 h(w)$ can assume values on either side of the interval $[\alpha_w^-, \alpha_w^+]$ where $\alpha_w^\pm = F(r_c^\pm)$, as was illustrated in Figure 3.2(A).

The equilibrium states of the whole system are given by the intersection in u, α_w space between $F(u)$ and the curve

$$\alpha_w(w(u)) \equiv \alpha_3 h(w), \quad w(u) = \alpha_4 g(u). \tag{3.11}$$

The curve $\alpha_w(w(u))$ is a monotonically decreasing function of u since $w(u)$ is a monotonically decreasing function of u and h is monotonic. In order for the slow subsystem to meet the above conditions, it is required that

$$\alpha_w(w(r_c^-)) > F(r_c^-), \quad \alpha_w(w(r_c^+)) < F(r_c^+). \tag{3.12}$$

This condition implies that $\alpha_w(w(u))$ and $F(u)$ must intersect for values of u where $F'(u) < 0$. Figure 3.3(A) illustrates the different scenarios that are possible for different values of the parameters of the slow subsystem. When the parameters are appropriately adjusted, the curves $\alpha_w(w(u))$ and $F(u)$ intersect once in the region where $F'(u) < 0$ and the conditions in (3.12) are satisfied. For other parameter values, there may be one, two, or three intersections of the curves, which violates one of the conditions in (3.12).

The limits of the inequalities in (3.12) can be used to obtain the regions in the parameter space, where the slow subsystem satisfies the required conditions. In particular, equation $\alpha_w(w(r_c^-)) = F(r_c^-)$ requires that $\alpha_w(w(u))$ and $F(u)$ intersect in the point where $F'(u) = 0$, i.e., in the maximum of the function $F(u)$. Hence, the critical values of the parameters where $\alpha_w(w(u))$ intersects an extremum of $F(u)$ satisfies the following condition:

$$\alpha_w(w(r_c^\pm)) = F(r_c^\pm), \quad F'(r_c^\pm) = 0. \tag{3.13}$$

We apply this condition to obtain the region in the (α_3, α_4) parameter plane for different values of η where the slow subsystem satisfies the requirements for relaxation oscillations. These curves are plotted in Figure 3.3(B) and show an increase of the oscillatory region (filled) with increasing η.

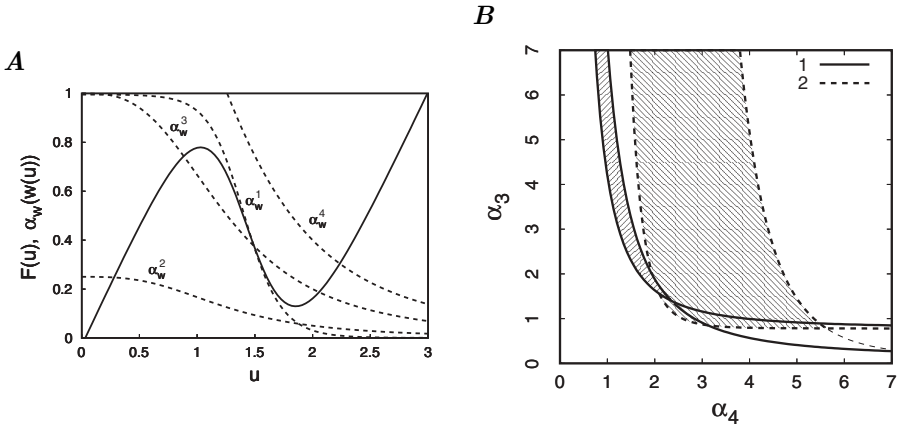

FIG. 3.3. *Geometrical analysis of equilibrium states as the parameters of the slow subsystem are varied.* (A) *Oscillations are possible* (3.12) *when the curves* $F(u)$ *and* $\alpha_w(w(u))$ *intersect only in the region where* $F'(u) < 0$ *(curve* α_w^1*,* $\eta = 4$*,* $\alpha_3 = 1$*,* $\alpha_4 = 3.8$*). The curves* α_w^2*,* α_w^3*, and* α_w^4 *are obtained for* $\eta = 1$*,* $\alpha_4 = 1$*, and* $\alpha_3 = 0.5$*, 2, 4, respectively. They illustrate monostability (*α_w^2 *and* α_w^4*) and multistability (*α_w^3*) in the system. Other parameters are* $\alpha_1 = 2$*,* $\alpha_2 = 4$*,* $\beta = \gamma = 3$*.* (B) *Regions in the* α_3*,* α_4 *parameter space where the conditions* (3.12) *are satisfied for different values of* η*:* (1) $\eta = 2$*;* (2) $\eta = 6$*.*

The condition in (3.13) is solved with respect to α_1 and α_2 (Appendix C) to give a set of bifurcation points (α_1^H, α_2^H) in the limit $\varepsilon = 0$:

$$\alpha_1^H(r) = \frac{1 + R_2(r)}{r - R_3(r)}, \quad \alpha_2^H(r) = (1 + r^\gamma)\,(R_2(r))^{1/\beta}, \tag{3.14}$$

where

$$\begin{aligned} R_2(r) =& \frac{\beta\gamma r^{\gamma-1}\,(r - R_3(r))}{(\beta\gamma r^\gamma - r^\gamma - \beta\gamma r^{\gamma-1} R_3(r) - 1)} - 1, \\ R_3(r) =& \alpha_3 \left(\frac{\alpha_4}{1 + r^\gamma}\right)^\eta \Bigg/ \left(1 + \left(\frac{\alpha_4}{1 + r^\gamma}\right)^\eta\right). \end{aligned} \tag{3.15}$$

As illustrated in Figure 3.4(A), the bifurcation curve has a loop structure and defines two distinct regions of parameter space. The region R is the set of α_1, α_2 values where system (3.1) can display oscillations for sufficiently low values of ε . The region labeled M defines a set of α_1, α_2 values where system (3.1) displays multistability.

3.3. Bifurcation analysis. The positions of equilibrium states $S = (u_0, v_0, w_0)$ in the full system in (3.1) are determined by the equations

$$\alpha_1 f(v_0) - u_0 + \alpha_3 h(w_0) = 0, \quad \alpha_2 g(u_0) - v_0 = 0, \quad \alpha_4 g(u_0) - w_0 = 0. \tag{3.16}$$

The stability of the equilibrium states are obtained from the Jacobian matrix,

$$J = \begin{pmatrix} -1 & \alpha_1 f_v'(v_0) & \alpha_3 h_w'(w_0) \\ \alpha_2 g_u'(u_0) & -1 & 0 \\ \varepsilon\alpha_4 g_u'(u_0) & 0 & -\varepsilon \end{pmatrix}, \tag{3.17}$$

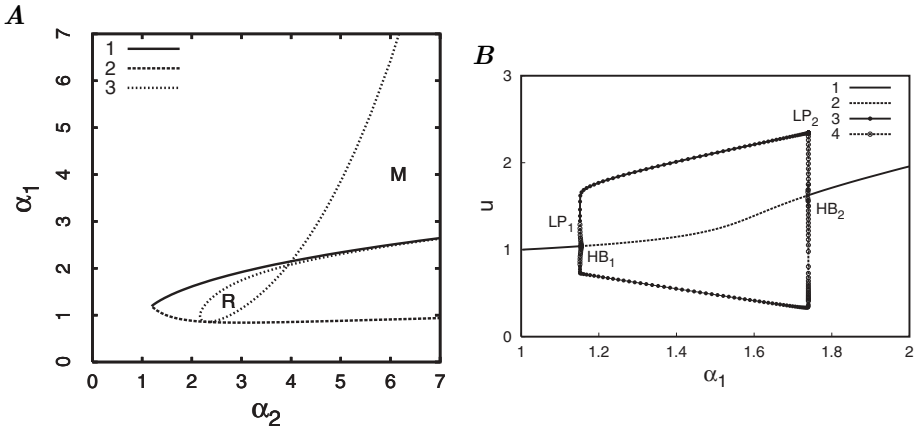

FIG. 3.4. *Bifurcation analysis of the full system.* (A) *Regions of different dynamic behavior in the* α_1, α_2 *parameter plane for* $\alpha_3 = 1, \alpha_4 = 3, \beta = \gamma = \eta = 3$. *Oscillations can occur in the region labeled R for sufficiently low* ε. *The system is bistable in the region labeled M and monostable everywhere else.* (B) *An example of bifurcation diagram obtained by variation in* α_1 *for a fixed value of* α_2 *(*$\alpha_2 = 3$*).*

by evaluation of the characteristic equation given by

$$\lambda^3 + \lambda^2(2+\varepsilon) + \lambda\left(1 - \alpha_1\alpha_2 f_v'(v_0)g_u'(u_0) + 2\varepsilon - \varepsilon\alpha_3\alpha_4 h_w'(w_0)g_u'(u_0)\right) + \varepsilon - \varepsilon\alpha_1\alpha_2 f_v'(v_0)g_u'(u_0) - \varepsilon\alpha_3\alpha_4 h_w'(w_0)g_u'(u_0) = 0. \tag{3.18}$$

The Andronov–Hopf bifurcation, which gives birth to a limit cycle, occurs when a pair of complex conjugate eigenvalues crosses the imaginary axis. If we write down the characteristic equation in the form $\lambda^3 + a\lambda^2 + b\lambda + c = 0$, then the condition for the Andronov–Hopf bifurcation takes the form $ab - c = 0$. From (3.18), this implies that the bifurcation occurs when the following condition is fulfilled:

$$1 - \alpha_1\alpha_2 f_v'(v_0)g_u'(u_0) + \varepsilon\left(2 - \frac{\alpha_3\alpha_4}{2} g_u'(u_0)h_w'(w_0)\right) + \varepsilon^2\left(1 - \frac{\alpha_3\alpha_4}{2} g_u'(u_0)h_w'(w_0)\right) = 0. \tag{3.19}$$

In the limit $\varepsilon \to 0$, we recover condition (3.13) for $\alpha_w(w(u))$ intersecting an extremum of $F(u)$. This is because a solution of the system (3.16), u_0, fits the equation $\alpha_w(w(u_0)) = F(u_0)$, and (3.19) for $\varepsilon = 0$ takes the form $1 - \alpha_1\alpha_2 f_v'(v_0)g_u'(u_0) = 0$, which is equivalent to $F'(u_0) = 0$. In other words, oscillations are constrained to be in the region where the conditions imposed by the slow subsystem (3.13) are satisfied, which, in turn, lies inside the region of hysteresis of the fast subsystem (Figure 3.2(B)).

Figure 3.4(B) illustrates in more detail the bifurcation structure of the full system when α_1 is varied at constant values of α_2. Here, Andronov–Hopf bifurcations, which correspond to entering and exiting from the oscillatory region, are labeled as HB_1 and HB_2. These bifurcations are subcritical and accompanied by saddle-node bifurcations of limit cycles LP_1 and LP_2. The points of Andronov–Hopf bifurcations agree well with the points of intersection of curve 3 of Figure 3.4(A) with the line that corresponds to the given value of α_2. This agreement shows that the region R in Figure 3.4(A) gives a good approximation for the oscillatory region of the full system if ε is small.

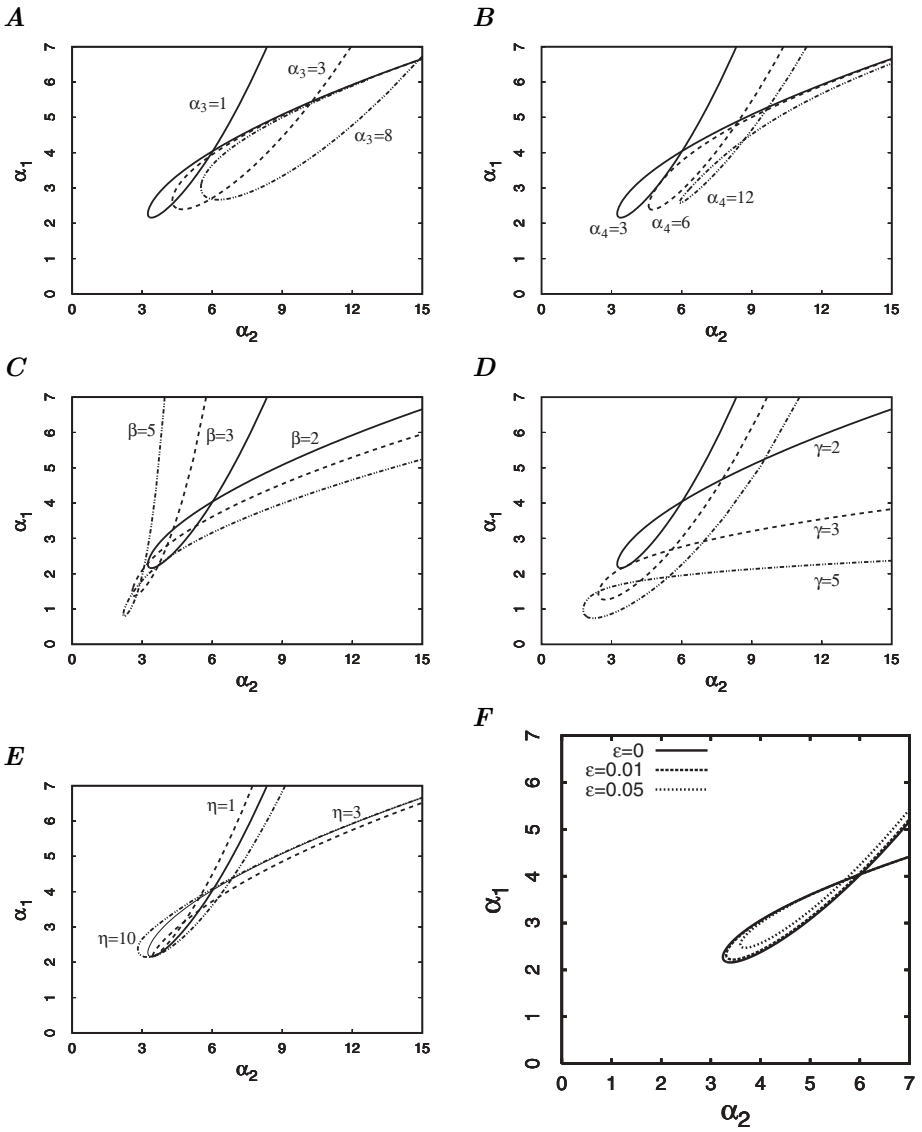

FIG. 3.5. *Increasing the oscillatory region in the α_1, α_2 parameter plane. All plots show the bifurcation curve $(\alpha_1^H(r), \alpha_2^H(r))$ for the reference parameters $\alpha_3 = 1$, $\alpha_4 = 3$, $\beta = \gamma = 2, \eta = 3$, $\varepsilon = 0$ in full. The six plots show the effect of variation in* (A) α_3, (B) α_4, (C) β, (D) γ, (E) η, *and* (F) ε *relative to the reference parameters.*

3.4. Parameter dependence. In this section we are optimizing conditions for oscillations by variation of all of the model parameters. In Figure 3.5(A)–(E), we plot the bifurcation curve $(\alpha_1^H(r), \alpha_2^H(r))$ defined in (3.14), i.e., for $\varepsilon = 0$. Increasing ε decreases the region in the α_1, α_2 parameter plane where oscillations are observed (Figure 3.5(F)). Comparing different curves in Figure 3.5(A), the range of both α_1 and α_2 values where oscillation can occur is seen to expand as α_3 is increased, indicating that larger values of α_3 increase the likelihood of oscillations. In Figure 3.5(B), it is seen that the region of oscillations is maximized at intermediate values of α_4. Therefore, the rate of AI synthesis must be carefully chosen to observe oscillations.

This can be done experimentally by manipulating the *luxI* RBS. Interestingly, Figure 3.5(C) shows a counterintuitive result, namely that the region of oscillations expands as β is decreased, i.e., when the degree of nonlinearity is decreased. Figure 3.5(D) and (E) shows the opposite effect for different nonlinearity exponents, namely that the oscillatory region shrinks when γ and η are decreased.

The exponents β and η have opposite influence because these two parameters change slopes of the function $F(u)$ and $a_w(u)$ independently. In the case where $a_w(u)$ coincides with the middle (decreasing) branch of $F(u)$, the system is very sensitive to changing other parameters. This is because very small variations of a parameter may cause an intersection outside the middle branch of $F(u)$, which corresponds to a stable equilibrium state. When the slope of $a_w(u)$ is less than of the middle branch of $F(u)$, relaxation oscillations cannot occur (see Figure 3.3, curve a_w^3). Thus, the larger the η, the larger the slope of $a_w(u)$, and the larger the tolerance of other parameters for oscillatory dynamics. By contrast, the larger the β, the larger the slope of $F(u)$, and the smaller the region of relaxation oscillations for given η. Parameter γ changes both $F(u)$ and $a_w(u)$, which results in an increase of the oscillatory region with increase of this parameter.

4. Oscillations in more detailed models. In this section, we consider how details left out during the derivation of the minimal model affect the ability of the single cells to display oscillatory behavior. We consider three important assumptions: (1) titration and saturation of the LuxR transcription factor by the AI, (2) two-step synthesis of the AI, and (3) the effect of "leaky" promoters. We also consider how oscillatory behavior can be made more robust by adding an additional connectivity to the network.

4.1. Taking LuxI synthesis into account increases the oscillatory region. As mentioned in the Introduction, the AI is not a gene product, but a small molecule synthesized by the protein encoded by the *luxI* gene (see Figure 1.1A). A more realistic description of the network would therefore involve production of AI in two steps, synthesis of the LuxI protein by the transcription and the translation of *luxI* and subsequent synthesis of the AI by the LuxI protein. This can be accounted for by introducing a new dimensionless variable, x, for the concentration of the LuxI protein and a rate of AI production that is proportional to x. The minimal model (3.1) is recovered when x is assumed to be in a quasi-steady state, $dx/d\tau = 0$. This assumption, however, is not justified since LuxI is a stable protein whose evolution occurs on the same time-scale as the slow variable w. Assuming the time-scales are the same, we take degradation rates of LuxI and AI to be equal and denote both of them as δ. When δ is small, the location of the oscillatory region is slightly shifted in the parameter space (data not shown), indicating that the model where LuxI synthesis is ignored, i.e., (3.1), is a reasonable approximation for this case. On the other hand, when δ is not small, the effect of time lag introduced by the two-step synthesis of the AI is significant. In the minimal model (3.1), oscillations are suppressed when the value of δ exceeds roughly 0.08 for all value of α_4. In the model that incorporates LuxI, oscillations cease when δ exceeds 0.3. This a major improvement for the likelihood of observing oscillations experimentally since smallness of the parameter δ is a major experimental challenge. It requires that the protein half-life, which typically is roughly 30 min or longer, is roughly 20 times shorter than the cell division time. Fortunately, the production of AI in two steps allows for a significant increase in the value of δ where oscillations can be observed. If other parameters are adjusted appropriately, it is possible to get oscillations for δ as high as 0.3.

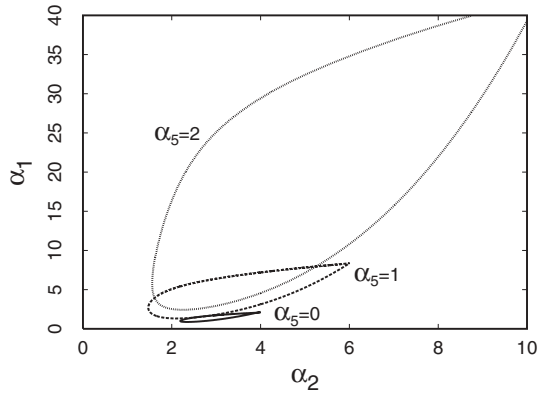

FIG. 4.1. *Increasing robustness of oscillations. The boundary of the oscillatory region in the α_1, α_2 parameter plane for different values of α_5. Parameter values: $\alpha_3 = 1$, $\alpha_4 = 0.03$, $\beta = \gamma = \eta = \zeta = 3$, $\delta = 0.01$, $D = 0$.*

4.2. Adding connectivity to the network increases the oscillatory region. The previous sections have demonstrated that the organization of oscillations in isolated cells requires that most of the parameters are precisely adjusted to a fairly narrow region of parameter space. We investigated if small changes to the system may enhance the region of parameter space where oscillations can be observed. One change that has a dramatic effect on the system is to express the gene coding for the V repressor from a promoter, denoted P_{W2}, that is repressed by AI.

$$\begin{aligned} \frac{du}{d\tau} &= \alpha_1 f(v) + \alpha_3 h(w) - u, \\ \frac{dv}{d\tau} &= \alpha_2 g(u) + \alpha_5 j(w) - v, \\ \frac{dw}{d\tau} &= \bar{\alpha}_2 g(u) - (\delta + D)w, \end{aligned} \tag{4.1}$$

where $\alpha_5 j(w) = \alpha_5/(1 + w^\zeta)$ represents expression of the protein V via the promoter P_{W2}. The model in (3.1) is recovered in the limit $\alpha_5 = 0$.

The addition of an AI-repressed promoter synthesizing the V repressor has a significant impact on the ability of isolated cells to oscillate since it favors the V high state in the absence of autoinducer without making the U high state harder to achieve in the presence of autoinducer. As a result, as α_5 increases, there is an increase in the region of parameter space where the fast subsystem has no stable equilibrium states and, thus, is able to oscillate. In Figure 4.1, we compare the region in the α_1, α_2 parameter plane where oscillations are observed for different values of α_5. It is evident that increased α_5 causes the region of oscillations to expand considerably, thus making oscillatory behavior in isolated cells more robust.

4.3. LuxR synthesis. As mentioned in the Introduction, the transcription factor that activates expression from the P_{lux} promoter is not the AI, as was assumed in the minimal model, but a complex comprised of LuxR and AI (Figure 1.1(A)). This complex is formed in a bimolecular reaction:

$$LuxR + AI \leftrightarrows LuxR - AI, \quad K_4 = \frac{k_{4f}}{k_{4b}}, \tag{4.2}$$

where K_4 is the equilibrium constant and k_{4b} and k_{4f} are the rate constants for the dissociation and association reaction, respectively. The *luxR* gene is assumed to be expressed at a constant rate from a plasmid-borne, constitutive promoter P_{con}, such that the LuxR protein is synthesized at a constant rate v_R. To obtain the minimal model (3.1), we need to assume here that the concentration of free autoinducer [AI] is negligible. That is, we assume that LuxR synthesis rate is large ($v_R \gg 1$) to provide LuxR for binding with AI, and the association reaction (4.2) is fast ($k_{4f} \gg k_{4b}$ and $k_{4f} \gg 1$). Our simulations reveal (data not shown) that, for smaller v_R, the oscillatory region shrinks and shifts to smaller α_1 and α_2. Violation of the other inequalities (e.g., $k_{4f} \ll k_{4b}$) makes the changes more significant. Hence, the details of formation of this effector complex may make oscillations more difficult to obtain.

4.4. Promoter leakage. In all of the models investigated, we have assumed that the promoters are fully repressible or fully silenced meaning that there is no expression from the promoter when repressor concentration is high or when activator is absent. In reality, many bacterial promoters are "leaky," and expression occurs at a basal level even under conditions where repressor is present in excess or activator is completely absent from the system.

To evaluate the effect of promoter leakage on the ability of isolated cells to oscillate, we introduced a constant synthesis term in each of the variables u and v that is proportional to maximal synthesis rate α_j. For simplicity, we use the same proportionality factor μ, corresponding to identical relative basal synthesis rates for all promoters. For large Hill coefficients $\eta = \zeta = 3$, the oscillations were observed at a fairly high value of leakage $\mu = 0.1$, i.e., 10% of the maximal synthesis rate for all promoters (data not shown). Decreasing the values of η and ζ causes the oscillatory region to be confined to lower values of μ. This indicates that organization of oscillations in isolated elements does not require the very tightly regulated promoters.

5. Ensemble of cells. We now study collective dynamics of the cell population. Introduction of coupling between elements of an ensemble can lead to qualitative changes of their dynamics. We are interested in providing synchronous oscillations, which would correspond to macroscopic oscillations of a protein concentration over the whole population. We demonstrate the possibility of both population synchronization and suppression of oscillations, depending on coupling strength and other parameters of the system.

First we make a transformation of the coordinates and parameters to combine intra- and extracellular degradation of the autoinducer into single term, thereby decreasing the number of parameters in the system. Then the system (2.14), describing the population of $i = 1, \dots, N$ cells, takes the form

$$
\begin{aligned}
\frac{du_i}{dt} &= \alpha_1 f(v_i) - u_i + \alpha_3 h(w_i),\\
\frac{dv_i}{dt} &= \alpha_2 g(u_i) - v_i,\\
\frac{dw_i}{dt} &= \bar{\varepsilon}\,(\bar{\alpha}_4 g(u_i) - w_i) + 2d(\bar{w}_e - w_i),\\
\frac{d\bar{w}_e}{dt} &= \frac{d_e}{N}\sum_{i=1}^{N}(w_i - \bar{w}_e).
\end{aligned}
\tag{5.1}
$$

Here, $\bar{w}_e = w_e\,(1 + \delta_e/D_e)$, $\bar{\varepsilon} = D + \delta - \frac{D}{(1+\delta_e/D_e)}$, $d = \frac{D}{2(1+\delta_e/D_e)}$, $d_e = D_e + \delta_e$, and $\bar{\alpha}_4 = \bar{\alpha}_2/\bar{\varepsilon}$.

Let us consider the simplest synchronous solution, i.e., identical synchronization of all elements of the ensemble: $u_i = u(t), v_i = v(t), w_i = w(t)$, $i = \overline{1,N}$. These equalities give the manifold of identity of corresponding coordinates: $M\{u_i, v_i, w_i : u_i = u_j, v_i = v_j w_i = w_j \forall i = \overline{1,N}, j = \overline{1,N}\}$. Now we study two matters: (1) dynamics on this manifold and (2) its stability. We show that if the isolated element displays relaxation oscillations, then the ensemble has the solution of identical synchronization for both small and large coupling strength. However, for the latter, the synchronous state may not be stable.

5.1. Identical synchronization. Dynamics on the manifold of identity of corresponding coordinates, M, is given by the following system:

$$\begin{aligned}
\frac{du}{dt} &= \alpha_1 f(v) - u + \alpha_3 h(w),\\
\frac{dv}{dt} &= \alpha_2 g(u) - v,\\
\frac{dw}{dt} &= \bar{\varepsilon}\,(\bar{\alpha}_4 g(u) - w) + 2d(\bar{w}_e - w),\\
\frac{d\bar{w}_e}{dt} &= d_e(w - \bar{w}_e).
\end{aligned} \tag{5.2}$$

Suppose that we have relaxation oscillations in each isolated element (for which $D_e \ll \delta_e$), i.e., we have the oscillations in this system with $d \to 0$ and $\bar{\varepsilon} \to \varepsilon = D + \delta$. We also assumed $\varepsilon \ll 1$ to obtain the oscillations.

We show first that the oscillations persist for small nonzero coupling strength $0 < d \ll 1$. We suppose also that the extracellular coupling coefficient is not small: $d_e \sim 1$. Then the system can be divided into fast and slow parts. The fast subsystem

$$\frac{du}{dt} = \alpha_1 f(v) - u + \alpha_3 h(w), \tag{5.3}$$

$$\frac{dv}{dt} = \alpha_2 g(u) - v, \tag{5.4}$$

$$\frac{d\bar{w}_e}{dt} = d_e(w - \bar{w}_e) \tag{5.5}$$

gives dynamics of three variables in the fast time-scale, where w is a constant. The u, v equations and the $\bar{w}_e$ equation do not depend on one another, so the fast subsystem splits into two independent parts. The u, v part is identical to the fast subsystem of the isolated element, in which all trajectories on the (u, v) plane converge to one of the equilibria. Trajectories of the $\bar{w}_e$ equation converge to the equilibrium state $\bar{w}_e = w$.

The slow subsystem is determined on the manifold of slow motion, i.e., in the intersection of all nullclines of the fast subsystem. This implies that we need to consider the equation for w on the manifold $\{\bar{w}_e = w, F(u) = \alpha_3 h(w)\}$. Substitution of the first constraint in the third equation of the system (5.2) gives

$$\frac{dw}{dt} = \bar{\varepsilon}(\bar{\alpha}_4 g(u) - w), \tag{5.6}$$

where u is a function of w, taken from the second constraint ($u = F^{-1}(\alpha_3 h(w))$). This equation has the same form as the slow equation obtained for the isolated element

(3.10), with parameters $\bar{\varepsilon}$ and $\bar{\alpha}_4$ representing other combinations of the initial parameters. Thus, for a given set of initial parameters D, δ, D_e, and δ_e, the slow dynamics of the system (5.2) with weak coupling strength d differs from the slow dynamics of the isolated element, but the parametric portrait of the isolated element with respect to parameters ε, α_4 coincides with the portrait for the system (5.2) with respect to parameters $\bar{\varepsilon}$ and $\bar{\alpha}_4$. If we have a solution for an isolated element with some values of ε and α_4, we can obtain the same solution in the system (5.2) with weak coupling strength d by tuning the parameters D, δ, D_e, and δ_e so that $\bar{\varepsilon}$ and $\bar{\alpha}_4$ take values ε and α_4. Thus, if a solution exists for the isolated element, then the same solution exists for the ensemble on the manifold of identical synchronization. Thus, we have shown, in particular, that there exists a regime of relaxation oscillations for a nonzero but weak coupling strength ($0 < d \ll 1$).

Next we consider the existence of a relaxation oscillation solution for large coupling strength $d \gg 1$. A shift in the frequency of the oscillation is obtained below for this case. The analysis can be performed analogously to that in [24]. There, the authors have proved that, for large coupling strength, the coupling term remains $O(1)$. Analogously, in our case, the coupling term $d(\bar{w}_e - w)$ is $O(\bar{\varepsilon})$ for large d, because the remaining part of the equation for w_i in system (5.2) is of that order (this follows from our analysis below). As $d \to \infty$, $w \to \bar{w}_e$, so $d(\bar{w}_e - w)$ is essentially a function of either one of the coordinates which enter the term. (This was proved rigorously in [24] for a related set of equations.) Using this, as in [24], we introduce $c(w) = d(\bar{w}_e - w)$.

We derive $\bar{w}_e$ from the definition of $c(w)$:

$$\bar{w}_e = w + \frac{1}{d} c(w). \tag{5.7}$$

Taking the derivative of this equation, we get

$$\frac{d\bar{w}_e}{dt} = \frac{dw}{dt}\left(1 + \frac{1}{d}\frac{dc(w)}{dw}\right). \tag{5.8}$$

Substituting this derivative and $c(w)$ into the third and fourth equation of system (5.2), we can rewrite them in the form

$$\frac{dw}{dt} = \bar{\varepsilon}(\bar{\alpha}_4 g(u) - w) + 2c(w), \tag{5.9}$$

$$\frac{dw}{dt}\left(1 + \frac{1}{d}\frac{dc(w)}{dw}\right) = -\frac{d_e}{d} c(w). \tag{5.10}$$

Excluding dw/dt from these equations, we get

$$[\bar{\varepsilon}(\bar{\alpha}_4 g(u) - w) + 2c(w)]\left(1 + \frac{1}{d}\frac{dc(w)}{dw}\right) = -\frac{d_e}{d} c(w). \tag{5.11}$$

The left-hand side of this equation is $O(\bar{\varepsilon})$. For a nonzero result in the leading order, $O(\bar{\varepsilon})$, we suppose that $\frac{d_e}{d} \sim 1$ and obtain

$$c_0(w) = -\frac{\bar{\varepsilon}(\bar{\alpha}_4 g(u) - w)}{2 + d_e/d}. \tag{5.12}$$

Note that we have not assumed $\bar{\varepsilon}$ small. The above result is valid for $\bar{\varepsilon} \sim 1$ whenever $d \gg \bar{\varepsilon}$.

Substituting $c_0(w)$ for $d(\bar{w}_e - w)$ in (5.2), we have the following three-dimensional system for synchronous oscillations in the limit of large coupling:

$$\begin{aligned} \frac{du}{dt} &= \alpha_1 f(v) - u + \alpha_3 h(w), \\ \frac{dv}{dt} &= \alpha_2 g(u) - v, \\ \frac{dw}{dt} &= \bar{\varepsilon} \frac{d_e}{2d + d_e} \left(\bar{\alpha}_4 g(u) - w \right). \end{aligned} \tag{5.13}$$

Hence, increasing the coupling strength d perturbs the parameter in front of the slow equation, changing the rate of change of the autoinducer, i.e., the slow timescale of the system. It follows from (5.11) that this perturbation is negligible if $d_e \gg d$ (to leading order $c(w) = 0$). But in the intermediate case $d_e \sim d$, the perturbation slows down the oscillations. In the limiting case $d_e \ll d$, (5.11) gives $c_0(w) = -\bar{\varepsilon}(\bar{\alpha}_4 g(u) - w)/2$, and, substituting $d(\bar{w}_e - w)$ in (5.2) by this formula, we obtain $dw/dt = o(\bar{\varepsilon})$. Thus, in the case $d_e \ll d$, the rate of change of the slow variable, w, is decreased by an order of magnitude, and so is the frequency of oscillations.

5.2. Stability of the synchronous solution. Now we examine stability of the solution obtained above with respect to small perturbations of the equalities of corresponding coordinates of the elements. We show that the synchrony may become unstable for large coupling strength. Let us define the perturbations in the following way: $u_i = u + \xi, u_j = u - \xi, v_i = v + \nu, v_j = v - \nu, w_i = w + \zeta, w_j = w - \zeta$, where i and j are any two numbers from 1 to N. Thus, we are perturbing any two elements of the ensemble in such a way that the perturbation does not affect the remaining elements. These perturbations are called transversal (or evaporational [25]) and test stability of the manifold of identical coordinates of the elements. The linearized equations for these perturbations are

$$\begin{aligned} \frac{d\xi}{dt} &= \alpha_1 f'(v)\nu - \xi + \alpha_3 h'(w)\zeta, \\ \frac{d\nu}{dt} &= \alpha_2 g'(u)\xi - \nu, \\ \frac{d\zeta}{dt} &= \bar{\varepsilon} \left(\bar{\alpha}_4 g'(u)\xi - \zeta \right) - 2d\zeta, \end{aligned} \tag{5.14}$$

where u, v, and w are taken in identity manifold with dynamics, governed by system (5.2). We solve this system numerically, calculating its Lyapunov exponents. They reveal stability of the synchronous solution with respect to the transversal perturbations and are therefore called transversal Lyapunov exponents. Figure 5.1 presents curves of the maximal transversal Lyapunov exponent vs. the coupling strength d for several sets of the other parameters. A negative value of the exponent implies transversal stability. The first curve corresponds to a set of parameters for which synchrony remains stable for any coupling strength. The second curve shows the maximal transversal Lyapunov exponent when only the parameter $\bar{\varepsilon}$ is changed. For this case, a fivefold increase in $\bar{\varepsilon}$ causes loss of stability with increasing coupling strength. The third curve illustrates the influence of another parameter on stability: changing α_1 shifts the manifold of slow motion so that the intersection with the nullcline of slow motion is shifted far apart from the extrema of the manifold. This shift makes the limit cycle more symmetric (see Figure 5.2) and leads to stability of this solution for any coupling strength even with a higher value of $\bar{\varepsilon}$, for which the oscillations are not

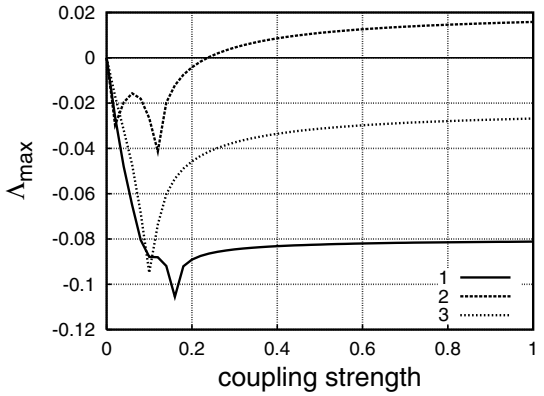

FIG. 5.1. *The largest transversal Lyapunov exponent vs. coupling strength for different sets of the parameters. Curve* (1) *corresponds to* $\bar{\varepsilon} = 0.01, \alpha_1 = 3$. *Curve* (2) *corresponds to* $\bar{\varepsilon} = 0.05, \alpha_1 = 3$, *so the nullclines are the same (see Figure* 5.2(A)*), and shows instability for large coupling strength. Curve* (3) *shows that oscillations can be stable even for such a high value of* $\bar{\varepsilon}$ *(*$\bar{\varepsilon} = 0.05$*) if the limit cycle is more symmetric (*$\alpha_1 = 3.2$ *as in Figure* 5.2(B)*).*

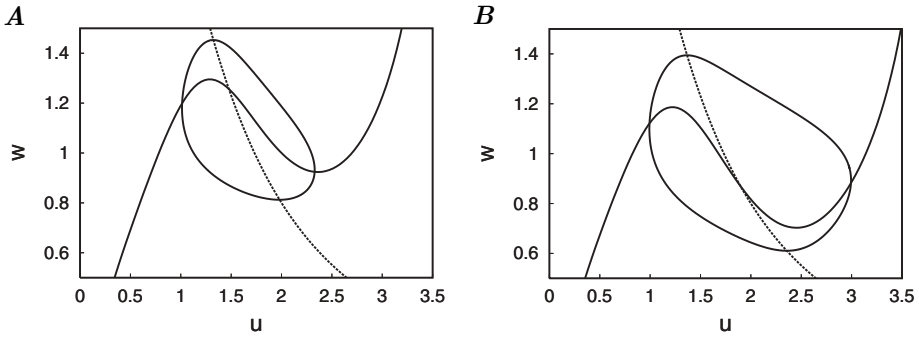

FIG. 5.2. *Position of the nullclines and form of limit cycles for* (A) *unstable and* (B) *stable synchrony. The only different parameter for these two cases is* α_1, *which is equal to* 3 *in the case* (A) *and* 3.2 *in the case* (B). *The other parameters are* $\alpha_2 = 5, \alpha_3 = 1, \bar{\alpha}_4 = 4, \beta = \gamma = \eta = 2$.

of relaxation type ($\bar{\varepsilon} = 0.05$). The illustrations of time series for the ensemble of 20 elements in the cases of stable and unstable identical synchronization solutions are presented in Figure 5.3. Thus, depending on the parameters of the element, we can keep the synchronous solution stable for any positive coupling strength or destabilize it for a large coupling strength.

The dependence of stability of a synchronous solution on parameters of the element can be explained qualitatively. The manifold of identical synchronization, M, has stable and unstable regions. Stability of a trajectory on this manifold is determined by the Lyapunov exponents, which measure whether perturbations decay or grow. As can be seen from computer simulations of this system, the perturbations grow during the fast motion, i.e., in the region, where u corresponds to the negative slope of the manifold of slow motion, $F'(u) < 0$ (see, e.g., Figure 5.2). By contrast, the perturbations decrease during the slow motion. If the time-scales are well separated, then the interval of time on the slow motion is much longer and contraction wins. Increasing $\bar{\varepsilon}$ leads to faster dynamics of the autoinducer (see (5.2)) and decreases intervals of time with slow motion. Thus, a synchronous solution may lose stability with

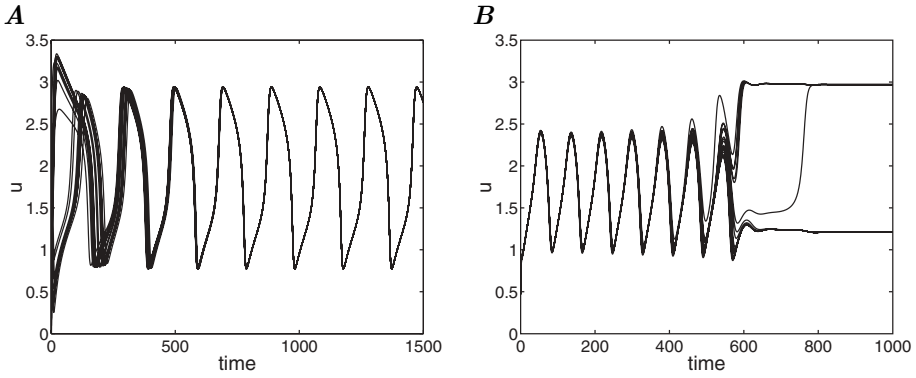

FIG. 5.3. *Examples of time series for the ensemble of* 20 *elements in the cases of* (A) *stable and* (B) *unstable synchronous solution.* $\alpha_1 = 3, \alpha_2 = 5, \alpha_3 = 1, \bar{\alpha}_4 = 4, \beta = \gamma = \eta = 2$*;* (A) $\bar{\varepsilon} = 0.01, d = 0.005$*;* (B) $\bar{\varepsilon} = 0.05, d = 0.3$.

respect to the transversal perturbations when dynamics of the autoinducer becomes faster.

The same argument can be applied to explain dependence of stability on the form of the limit cycle. Given the same time separation ($\bar{\varepsilon}$) for both trajectories in Figure 5.2, in the case (A), the major part of the trajectory lies in the middle region of u, where $F'(u) < 0$. Here, the transversal perturbations grow, giving divergence of the close trajectories from the limit cycle. In the case (B), the limit cycle has much larger parts outside the middle region, which contributes to the decrease of the perturbations and causes convergence in average along the limit cycle.

5.3. Stable equilibria for large coupling strength. In this section we show that large diffusion may cause emerging steady states of the protein concentrations and ceasing of the oscillations in the population. We are going to show existence and stability of new equilibria in the phase space of the ensemble (5.1) for large coupling strength. Taking into account our result on synchronization of this population, the new equilibria may coexist with the stable synchronous periodic solution, dividing the phase space into basins of attraction.

We conduct the analysis analogous to [26] and [27]. Consider for simplicity a pair of the elements

$$
\begin{aligned}
\frac{du_1}{dt} &= \alpha_1 f(v_1) - u_1 + \alpha_3 h(w_1),\\
\frac{dv_1}{dt} &= \alpha_2 g(u_1) - v_1,\\
\frac{dw_1}{dt} &= \bar{\varepsilon}\,(\bar{\alpha}_4 g(u_1) - w_1) + 2d(\bar{w}_e - w_1),\\
\frac{du_2}{dt} &= \alpha_1 f(v_2) - u_2 + \alpha_3 h(w_2),\\
\frac{dv_2}{dt} &= \alpha_2 g(u_2) - v_2,\\
\frac{dw_2}{dt} &= \bar{\varepsilon}\,(\bar{\alpha}_4 g(u_2) - w_2) + 2d(\bar{w}_e - w_2),\\
\frac{d\bar{w}_e}{dt} &= \frac{d_e}{2}(w_1 + w_2 - 2\bar{w}_e).
\end{aligned}
\tag{5.15}
$$

Equilibrium states of the system are given by

$$\begin{aligned}
\alpha_1 f(v_1) - u_1 + \alpha_3 h(w_1) &= 0,\\
\alpha_2 g(u_1) - v_1 &= 0,\\
\bar{\varepsilon}(\bar{\alpha}_4 g(u_1) - w_1) + 2d(\bar{w}_e - w_1) &= 0,\\
\alpha_1 f(v_2) - u_2 + \alpha_3 h(w_2) &= 0,\\
\alpha_2 g(u_2) - v_2 &= 0,\\
\bar{\varepsilon}(\bar{\alpha}_4 g(u_2) - w_2) + 2d(\bar{w}_e - w_2) &= 0,\\
w_1 + w_2 - 2\bar{w}_e &= 0.
\end{aligned} \tag{5.16}$$

Again, we derive v_i from these equations as $v_i = \alpha_2 g(u_i)$, and substituting them into the remaining equations, we can write u_i as a function of w_i: $u_i = F^{-1}(\alpha_3 h(w_i))$, where, as before, $F(u) = u - \alpha_1 f(\alpha_2 g(u))$. The extracellular autoinducer concentration can also be presented as a function of w_i: $\bar{w}_e = (w_1 + w_2)/2$. Since u_i, v_i, and $\bar{w}_e$ are determined by w_i, the equilibria of the system can be found from a two-dimensional system presented in the following form:

$$\begin{aligned}
w_2 &= w_1 - \frac{\bar{\varepsilon}}{d} R(w_1),\\
w_1 &= w_2 - \frac{\bar{\varepsilon}}{d} R(w_2),
\end{aligned} \tag{5.17}$$

where

$$R(w) = \bar{\alpha}_4 g\left(F^{-1}(\alpha_3 h(w))\right) - w. \tag{5.18}$$

This system gives two curves in the (w_1, w_2) plane, intersections of which correspond to equilibria of the pair of elements.

Consider the case where each isolated element displays relaxation oscillations. In particular, let us take the same parameters of the element as in Figure 5.2(A). The curves given by system (5.17) are shown in Figure 5.4 for two different values of the coupling parameter d. Here, with increasing coupling strength, two new intersections of these curves emerge. The intersections correspond to equilibria, the stability of which is shown below.

To explain the emergence of the new equilibria, we divide the dynamics of the system into fast and slow motion, taking $\bar{\varepsilon} \sim d \ll 1$. Consider first the fast subsystem of system (5.15):

$$\begin{aligned}
\frac{du_1}{dt} &= \alpha_1 f(v_1) - u_1 + \alpha_3 h(w_1),\\
\frac{dv_1}{dt} &= \alpha_2 g(u_1) - v_1,\\
\frac{du_2}{dt} &= \alpha_1 f(v_2) - u_2 + \alpha_3 h(w_2),\\
\frac{dv_2}{dt} &= \alpha_2 g(u_2) - v_2,\\
\frac{d\bar{w}_e}{dt} &= \frac{d_e}{2}(w_1 + w_2 - 2\bar{w}_e),
\end{aligned} \tag{5.19}$$

where w_1 and w_2 can be taken to be constant ($\dot{w}_1 = \dot{w}_2 = 0$) and equal to their initial values. This system has three independent parts: for (u_1, v_1), (u_2, v_2), and for $\bar{w}_e$

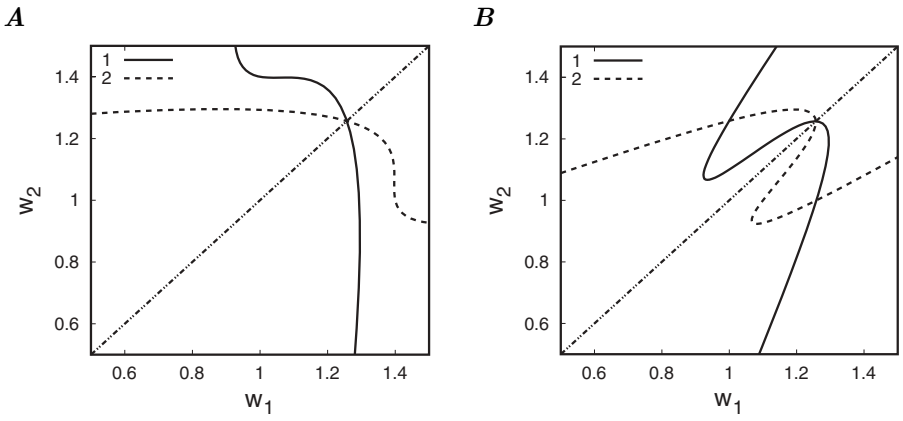

FIG. 5.4. *Equilibrium states of the pair of elements are in the points of intersection of the two curves given by system* (5.17)*, which are plotted for* (A) $\bar{\varepsilon}/d = 2$*;* (B) $\bar{\varepsilon}/d = 0.5$*. Curves* 1 *and* 2 *correspond to the first and the second equations in* (5.17)*. The dashed diagonal line is the manifold of identity of the w coordinates. In case* (B) *we have two intersections of the nullclines outside the diagonal, which are stable equilibria.*

(each part does not include variables from other parts). The equation for $\bar{w}_e$ has the equilibrium $\bar{w}_e = (w_1 + w_2)/2$, which is stable. The remaining two systems for (u_i, v_i) coincide with the fast subsystems for the isolated element (3.2), i.e., the elements are effectively uncoupled with respect to fast motion. Hence, these systems cannot have closed orbits. The only trajectories which attract or repel all others nearby are equilibrium states, defined, as before, by

$$-F(u_i) + \alpha_3 h(w_i) = 0, \qquad v_i = \alpha_2 g(u_i), \quad i = 1, 2. \tag{5.20}$$

The position of the equilibria, depending on w_i, constitutes the manifold of slow motion for the whole system (5.15), where the fast equations do not contribute to the motion, and the motion is governed entirely by the slow subsystem. The manifold for each of the elements of the coupled system (5.15) is given by the same curve (Figure 5.5), which is identical to the one obtained for the isolated element (3.2). Figure 5.5 shows trajectories for the two elements from their initial conditions $(u_1, \alpha_{w,1})$ and $(u_2, \alpha_{w,2})$, where $\alpha_{w,i} = \alpha_3 h(w_i)$. Once the elements come to their manifolds of slow motion, fast motion ceases and the trajectory moves along the manifold, governed by the slow subsystem

$$\begin{aligned} \frac{dw_1}{dt} &= \bar{\varepsilon}\,(\bar{\alpha}_4 g(u_1) - w_1) + d(w_2 - w_1), \\ \frac{dw_2}{dt} &= \bar{\varepsilon}\,(\bar{\alpha}_4 g(u_2) - w_2) + d(w_1 - w_2), \end{aligned} \tag{5.21}$$

where $u_i = F^{-1}(\bar{\alpha}_4 h(w_i)), i = 1, 2$. For $d = 0$, w_i increases along the left-hand branch of $F(u)$ and decreases on the right-hand branch. In the case plotted in Figure 5.5, by providing attraction of the w_i coordinates to each other, the coupling term speeds up motion along the manifold until $w_1 = w_2$. After that, the coupling slows down the motion. If the coupling strength is high enough, it can stop the motion along the manifold, compensating for the slow dynamics of the individual elements, as plotted in Figure 5.5.

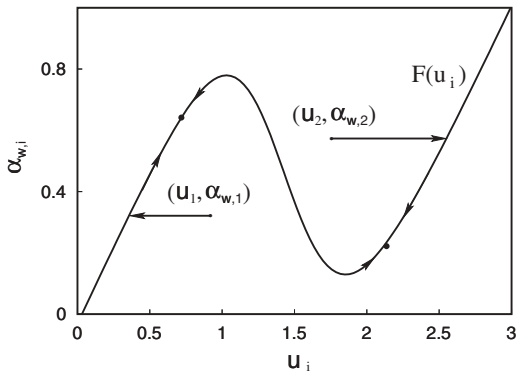

FIG. 5.5. *Fast motion in the pair of elements. The manifolds of slow motion for these two elements coincide with each other. The fast motion attracts the trajectory to one of the outer branches of the manifold. The middle branch is unstable with respect to fast motion.*

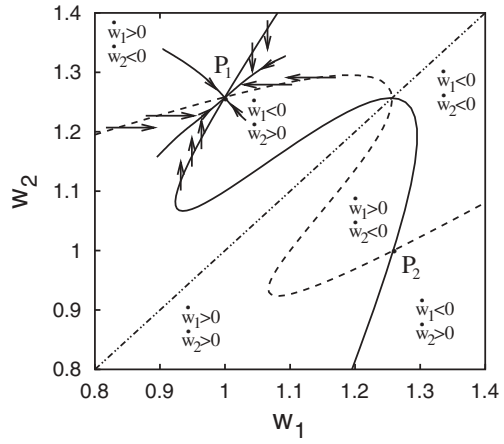

FIG. 5.6. *Phase diagram of slow system* (5.22) *near equilibria* P_1 *and* P_2.

5.4. Stability of the new equilibria. We are going to show that the equilibrium states are stable with respect to both fast and slow motion. Consider first the slow subsystem (5.21), which, using the function $R(w)$ defined in (5.18), can be presented as

$$\begin{aligned} \frac{dw_1}{dt} &= \bar{\varepsilon} R(w_1) + d(w_2 - w_1), \\ \frac{dw_2}{dt} &= \bar{\varepsilon} R(w_2) + d(w_1 - w_2). \end{aligned} \tag{5.22}$$

The curves (5.17), plotted in Figure 5.4, are nullclines of this system. Determining the sign of $\dot{w}_1$ and $\dot{w}_2$ from (5.22) in different regions of the (w_1, w_2) plane, we can qualitatively plot directions of trajectories for the slow subsystem. This gives us the picture in Figure 5.6, which shows stability with respect to slow motion of the equilibrium states P_1 and P_2.

Next consider stability with respect to the fast motion. We know that, in the singular limit $\bar{\varepsilon} \to 0$, the middle branch of the manifold of slow motion for the isolated element is unstable (Figure 5.5). Even in the case when there is an equilibrium in the middle branch and the slow motion converges to it, the fast motion provides divergence (see Figure 3.2(A) curve α_{w3}). Thus, we can determine stability of an equilibrium state with respect to the fast motion based only upon its position on the manifold of slow motion. In particular, if the equilibrium state is situated in the middle branch of the manifold, then it is unstable.

This rule helps us to determine stability of the equilibria in the intersections of the curves in the (w_1, w_2) plane (Figure 5.4). The curves have three monotonic branches, which correspond to the branches of the manifold of slow motion, given by $F(u)$. The middle branch of the manifold, which is unstable with respect to fast motion, corresponds to the middle branch of the curves $w_1(w_2)$ and $w_2(w_1)$. Hence, the equilibrium state in the diagonal in Figure 5.4(A) and (B) is unstable, but the pair of new equilibria in Figure 5.4(B) is stable with respect to fast motion. This suggests the new equilibrium states are stable for large coupling strength.

Stability of the equilibria can be shown rigorously by the standard characteristic equation method. The characteristic equation for the pair of interacting elements (5.15) can be written in the following form:

$$\Omega_1\Omega_2(-d_e-\lambda) - \Omega_1\Delta_2 d_e d - \Omega_2\Delta_1 d_e d = 0. \tag{5.23}$$

Here, $\Delta_i = (1+\lambda)^2 - \alpha_2 g'(u_i)\alpha_1 f'(v_i)$, $\Omega_i = \Delta_i(-\bar{\varepsilon}-2d-\lambda)+(1+\lambda)\alpha_3 h'(w_i)\bar{\varepsilon}\alpha_4 g'(u_i)$. This is a seventh order equation with respect to λ.

To carry out stability analysis for the case considered above in a more rigorous way, we suppose $d \sim \bar{\varepsilon} \ll 1$. We are looking first for eigenvalues of the order one, $\lambda \sim 1$. To leading order of magnitude, (5.23) gives

$$\Delta_1\Delta_2\lambda^2(-d_e-\lambda) = 0.$$

The first root of this equation is $\lambda_1 = -d_e$; the other four roots, $\lambda_{2,3}$ and $\lambda_{4,5}$, come from the quadratic equations $\Delta_1 = 0$ and $\Delta_2 = 0$, respectively. All of them are negative if $1 - \alpha_2 g'(u_i)\alpha_1 f'(v_i) > 0$, which is equivalent to $F'(u_i) > 0$ (see section 3.3). The remaining two eigenvalues, $\lambda_{6,7}$, obtained from this equation are zero. We need to consider a lower order of magnitude of equation (5.23) to determine their signs. Thus next we suppose $\lambda \sim \bar{\varepsilon}$. Then the leading order of (5.23) is $O(\bar{\varepsilon}^2)$:

$$\begin{aligned}
&\Big[F'(u_1)(-\bar{\varepsilon}-2d-\lambda) + \bar{\varepsilon}\alpha_3 h'(w_1)\alpha_4 g'(u_1)\Big] \\
&\quad\times\Big[F'(u_2)(-\bar{\varepsilon}-2d-\lambda) + \bar{\varepsilon}\alpha_3 h'(w_2)\alpha_4 g'(u_2)\Big](-d_e) \\
&\quad-\Big[F'(u_1)(-\bar{\varepsilon}-2d-\lambda) + \bar{\varepsilon}\alpha_3 h'(w_1)\alpha_4 g'(u_1)\Big]F'(u_2)d_e d \\
&\quad-\Big[F'(u_2)(-\bar{\varepsilon}-2d-\lambda) + \bar{\varepsilon}\alpha_3 h'(w_2)\alpha_4 g'(u_2)\Big]F'(u_1)d_e d = 0,
\end{aligned} \tag{5.24}$$

where we take only $O(1)$ terms in Δ_i and $O(\bar{\varepsilon})$ terms in Ω_i. This is a quadratic equation, which can be written in the form $a\lambda^2 + b\lambda + c = 0$ with the coefficients $a = -F'(u_1)F'(u_2)$, $b = -2(\bar{\varepsilon}+d)F'(u_1)F'(u_2)+\bar{\varepsilon}\alpha_3\alpha_4[F'(u_1)h'(w_2)g'(u_2)+F'(u_2)\times h'(w_1)g'(u_1)]$, $c = -(\bar{\varepsilon}+2d)\bar{\varepsilon}F'(u_1)F'(u_2) + (\bar{\varepsilon}+d)\bar{\varepsilon}\alpha_3\alpha_4[F'(u_1)h'(w_2)g'(u_2)+F'(u_2)h'(w_1)g'(u_1)] - \bar{\varepsilon}^2\alpha_3^2\alpha_4^2 h'(w_1)h'(w_2)g'(u_1)g'(u_2)$. We need to show that $\lambda_{6,7} = (-b \pm \sqrt{b^2-4ac})/2a$ are negative or, equivalently, that $-b \pm \sqrt{b^2-4ac} > 0$. Consider the region where all the eigenvalues of the leading order, $O(1)$, are negative, i.e.,

$F'(u_i) > 0$. Then it is obvious that the first coefficient, a, is negative. All three terms of c coefficient are negative because $h'(w_i) \geq 0$ and $g'(u_i) \leq 0$ everywhere. Thus, $ac > 0$, $b^2 - 4ac < b^2$, or $\sqrt{b^2 - 4ac} < |b|$. The coefficient b is also negative; hence the latter inequality gives $\sqrt{b^2 - 4ac} < -b$, or $-b - \sqrt{b^2 - 4ac} > 0$. Thus, all eigenvalues are negative under conditions $F'(u_i) > 0$, showing stability of the equilibria in the outer branches of the function $F(u)$.

Analogously, one can show stability of the equilibria for the case of large or moderate coupling strength d.

5.5. Impact of the collective dynamics. We now discuss how requirements for obtaining oscillations are changed in the case of a population of interacting cells. One of the key experimental problems is to achieve a sufficiently slow dynamics of the autoinducer. The time-scale of autoinducer dynamics is determined by the coefficient in front of the right part of the equation for autoinducer concentration—a rate constant. For the isolated element (3.1), this coefficient is ε; for the system on the manifold of identical synchronization (5.2), it is $\bar{\varepsilon}$. We have shown that the lower the rate constant (the slower dynamics of autoinducer) the larger the oscillatory region (see Figure 3.5(F)). For population dynamics, the rate constant depends on the coupling strength (see, e.g., (5.13)). It follows from (5.11) that the autoinducer dynamics is much slower than in isolated element if $d_e \ll d$ and $d \gg \bar{\varepsilon}$. Hence, we can slow down dynamics of the autoinducer using properties of the collective dynamics. The assumption that $d_e \ll d$ ($d = \frac{D}{2(1+\delta_e/D_e)}$, $d_e = D_e + \delta_e$) is quite plausible for the experiment because D_e is presented usually as $D_e = \frac{D\rho}{1-\rho}$, where ρ is cell density, and $\rho \ll 1$. Then $D_e \ll D$, and if we suppose that $\delta_e \sim D_e$, we come to the inequality $d_e \ll d$. The other assumption ($d \gg \bar{\varepsilon}$) is also plausible because the permeability of the cell membrane to the autoinducer molecules is expected to be relatively high ($D \gg 1$).

Stability of the synchronous solution also depends on the time-scale of the autoinducer dynamics. We have shown that synchrony may be stable for a small rate constant $\bar{\varepsilon}$ and unstable for larger $\bar{\varepsilon}$ (see Figure 5.1). Those computations were made for $d_e \gg d$ so that the period of oscillations was not changed significantly with increasing coupling strength. Now, if $d_e \ll d$, increasing coupling strength also slows down the oscillations (5.13), causing stabilization of the synchronous solution (data not shown).

On the other hand, increasing coupling strength also causes emergence of the new equilibria. The higher the coupling strength, the larger the domains of attraction of the new equilibria and the larger the probability of obtaining a steady state instead of synchronous oscillations in the experiment. The effect is very strong because the coupling strength sufficient for the formation of the equilibria is of the same order of magnitude as $\bar{\varepsilon}$. To avoid formation of the equilibria, we need to keep $\bar{\varepsilon}$ larger than d, which contradicts the conditions used above. Thus, our theoretical study of the simplified model (5.1) predicts a potential problem for the experimental implementation of the synchronous oscillatory dynamics.

6. Solving experimental problems (discussion). In this section we summarize the results of our investigations and discuss the conditions required for population synchronous oscillations in the light of constraints imposed by experimental considerations. Our study of a simplified model shows that population synchronous oscillations are theoretically possible. However, there may be some difficulties in achieving population synchronous oscillations experimentally. First of all, a strong

interaction between cells (e.g., high permeability of the membrane to the autoinducer) may result in the suppression of synchronous oscillations and a transition to a stable heterogeneous population state where individual cells are locked in different stable equilibrium states. On the other hand, if the cell-to-cell interactions are too weak, individual cells may oscillate but will be unable to achieve synchrony. Therefore, the parameters that determine the coupling strength between cells must be finely adjusted. Cell-to-cell variations in parameter values and initial conditions increase the likelihood that the population synchronous oscillation will be suppressed. As our study has shown, mere difference in initial conditions for different cells may be sufficient to obtain a stationary population state and suppression of individual cellular oscillators, even though the synchronous solution is asymptotically stable.

Fortunately, the system provides a possibility for attracting a very broad distribution of initial conditions to the synchronous solution. This requires the dynamics of the extracellular autoinducer to be much slower than the intracellular ones, which corresponds to the condition $d_e \ll d$ discussed in the end of the previous section. In this case (and for large coupling strength d), the motion from the initial conditions starts with relaxation of the concentrations of the intracellular autoinducer in different cells toward the state where the concentrations are equal to the extracellular concentration. If the extracellular autoinducer is washed out at the onset of the experiment, then the initial state will have the extracellular concentration that is close to zero. Thus, the concentrations inside the cells approach a low value. Once the low concentration has been achieved, the concentrations of the repressor proteins inside all cells approach the same state: low u and high v. This state is in the domain of attraction of the synchronous solution, and synchrony can be achieved even when other attractors exist.

Moreover, if the parameters of individual cells are different, the identical synchronization solution does not exist at all. Our computational study of the model of the population shows that the introduction of inhomogeneity in parameters increases the probability of obtaining a stationary state starting from random initial conditions. Generally speaking, a larger variation in the parameter values of individual elements (e.g., a larger difference in the individual cellular oscillators and high cell-to-cell variability) will decrease the likelihood of observing a population synchronized oscillatory state. This is particularly important since many engineered gene regulatory networks, including the toggle switch and the Lux-based cell-to-cell communication system, are carried on self-replicating plasmids. The number of plasmids per cell (and hence the number of genes and promoters they carry) is know to vary quite dramatically [20], and it will probably be necessary to minimize this source of cell-cell variability in order to achieve population synchronous oscillations. This could be achieved by using plasmids with more elaborate mechanisms of copy-number and partitioning control or by integrating the engineered network into the bacterial chromosome.

In addition to parameter differences caused by fluctuations in the number of genes per cell, there are other sources of cell-to-cell variability that cannot easily be minimized. These include variation in growth rates, differences in the concentration of polymerases and of ribosomes, and others. Moreover, genetic manipulations usually introduce rather coarse changes, and it is generally difficult to fine-tune the parameter values that govern the dynamics of individual cells. Therefore, to increase the likelihood of population synchronous oscillations, it is important to have a rather large parameter region where oscillatory dynamics for the isolated element is observed.

We have shown that this can be achieved by increasing the maximal rate (α_3)

of synthesis of one of the repressors (u) from the promoter that is regulated by the autoinducer. The expansion of the oscillatory region also requires an increase of the maximal rate (α_2) of synthesis of the second repressor (v). Our investigation indicates that an increased nonlinearity, i.e., the parameters for promoter cooperativity β, γ, and η, does not significantly expand the region of parameter space where oscillations in isolated elements can be observed. Increasing the value of β (cooperativity for promoter that synthesizes u repressor) actually causes a contraction of the oscillatory region. In addition, to achieve the largest oscillatory region possible, the rate of decay of the autoinducer ε must be as small as possible (of a smaller order of magnitude, $\varepsilon \ll 1$). This may pose an experimental challenge because it implies that the rates of autoinducer synthesis ($\varepsilon \times \alpha_4$) and decay ($\varepsilon$) are at least an order of magnitude lower than the rates of the repressors synthesis (α_1 and α_2) and decay (which is equal to 1). While the maximal rate of autoinducer synthesis could be made low by genetic manipulations, the rate of decay is primarily determined by dilution due to the cell growth. This dilution of course affects all cellular components identically. Moreover, the autoinducer is able to penetrate the cell membrane, and the value of the rate parameter ε depends linearly on the diffusion coefficient D of the autoinducer, which may be large.

For mathematical tractability, our simplified model ignores the fact that the synthesis of the autoinducer is a two-step process that requires the synthesis of the protein LuxI. Taking this step into consideration partially solves the problem with the smallness of ε. First, the additional step introduces a delay in production of the autoinducer. Second, the degradation rate of LuxI is the same as that of the repressors since the LuxI protein is unable to penetrate the cell membrane. As shown by numerical simulations, it is possible to achieve oscillations when the decay rate of the autoinducer is only three times smaller than the decay rates of the repressor proteins. This is in contrast to the simplified model, where an order of magnitude difference was required. In other words, the simplified model may actually underestimate the likelihood of achieving oscillatory dynamics. Further improvement of the gene network toward the ability to oscillate was achieved by the introduction of a promoter that is repressible by the autoinducer and synthesizes protein v, i.e., a negative feedback from the autoinducer to one of the repressors (see section 4.2). Such a promoter has previously been described in the literature [28]. Our simulations demonstrate that the oscillatory region can be substantially increased when this negative feedback is added. It is our belief that this slight variation in the architecture of gene regulatory network would be very useful experimentally as it increases the robustness of single-cell oscillations quite dramatically.

The problem of new equilibria also can be overcome in the experiment if we take into account the LuxI synthesis step and/or introduce the additional network connectivity. In the simplified model, the degradation rate constant of the autoinducer $\bar{\varepsilon}$ must be larger than the coupling coefficient d to avoid the presence of equilibria. On the other hand, $\bar{\varepsilon}$ must be small to provide relaxation type of oscillations, and d must be large enough to synchronize the ensemble. This contradiction is resolved if the second slow process, LuxI synthesis, is taken into account. This introduces an additional delay in production of the autoinducer and allows the rate constants of the autoinducer to take higher values without losing the oscillations. Moreover, these rate constants are expected to take much higher values than the rate constants of the LuxI synthesis because the effective rate of degradation for the autoinducer includes the diffusion coefficient D ($\bar{\varepsilon}_w = D + \delta - \frac{D}{(1+\delta_e/D_e)}$), but the rate of degradation

for LuxI does not ($\bar{\varepsilon}_x = \delta$). Hence, the LuxI dynamics has the function of slowing down the oscillations; its rate constant must be several times smaller than those of the other proteins. The rate constants of the autoinducer can be chosen large enough so that the degradation rate constant is larger than the coupling coefficient: $\bar{\varepsilon}_w > d$. Thus, it is theoretically possible to simultaneously achieve absence of the equilibria and strongly enough attracting synchronous oscillations.

Appendix. Derivation of parametric formula for approximations of bifurcation boundaries.

Appendix A. The saddle-node bifurcation for the toggle switch. We are solving the system which gives the curve of the saddle-node bifurcation for the fast subsystem in the absence of the autoinducer:

$$F(u) = 0, \qquad F'(u) = 0.$$

Substituting the function $F(u)$, defined as (3.3), we can rewrite it in the form

$$\frac{\alpha_1}{1+\left(\frac{\alpha_2}{1+u^\gamma}\right)^\beta} = u, \qquad \left(1+\left(\frac{\alpha_2}{1+u^\gamma}\right)^\beta\right)^2 = \left(\frac{\alpha_2}{1+u^\gamma}\right)^\beta \frac{\alpha_1\beta\gamma u^{\gamma-1}}{1+u^\gamma}. \tag{A.1}$$

We define $R = (\frac{\alpha_2}{1+u^\gamma})^\beta$. From the first equation of the latter system, we have $R = \frac{\alpha_1}{u} - 1$. Using this combination in the second equation of system (A.1), we obtain

$$\left(\frac{\alpha_1}{u}\right)^2 = \left(\frac{\alpha_1}{u} - 1\right)\frac{\alpha_1\beta\gamma u^{\gamma-1}}{1+u^\gamma}, \tag{A.2}$$

or

$$\alpha_1 = \frac{\beta\gamma u^{\gamma+1}}{\beta\gamma u^\gamma - (1+u^\gamma)}. \tag{A.3}$$

R has appeared to be a function of u and depends on γ and β, but it does not depend on α_1 and α_2:

$$R(u) = \frac{\beta\gamma u^\gamma}{\beta\gamma u^\gamma - (1+u^\gamma)} - 1. \tag{A.4}$$

Then, from the definition of R, we have

$$\alpha_2 = (R(u))^{1/\beta}(1+u^\gamma). \tag{A.5}$$

We introduce a parameter $r > 0$, replacing u in the obtained formulas, to show that we have obtained a bifurcation boundary in the space (α_1, α_2) parametrized by an independent parameter. The resulting formulas of the saddle-node bifurcation curve for the fast subsystem in absence of the autoinducer are

$$\begin{aligned} \alpha_1^c &= \frac{\beta\gamma r^{\gamma+1}}{1+r^\gamma} \Big/ \left(\frac{\beta\gamma r^\gamma}{1+r^\gamma} - 1\right), \\ \alpha_2^c &= (1+r^\gamma)\left(\frac{\beta\gamma r^\gamma}{1+r^\gamma} \Big/ \left(\frac{\beta\gamma r^\gamma}{1+r^\gamma} - 1\right) - 1\right)^{1/\beta}. \end{aligned} \tag{A.6}$$

Appendix B. Merging extrema of the function $F(u)$. We have the following condition for merging extrema of a function:

$$F^{'}(u) = 0, \quad F^{''}(u) = 0,$$

which, in our case, takes the form

$$\left(1 + \left(\frac{\alpha_2}{1+u^\gamma}\right)^\beta\right) = \left(\frac{\alpha_2}{1+u^\gamma}\right)^\beta \frac{\alpha_1\beta\gamma u^{\gamma-1}}{1+u^\gamma},$$

$$\left(\frac{\alpha_2}{1+u^\gamma}\right)^\beta = -\frac{(\gamma-1) - u^\gamma(1+\beta\gamma)}{(\gamma-1) + u^\gamma(\beta\gamma-1)}. \tag{B.1}$$

We define $R = (\frac{\alpha_2}{1+u^\gamma})^\beta$. From the second equation of the latter system, we have

$$R = -\frac{(\gamma-1) - u^\gamma(1+\beta\gamma)}{(\gamma-1) + u^\gamma(\beta\gamma-1)}. \tag{B.2}$$

This formula shows again that R has appeared to be a function of u, which depends on γ and β, but does not depend on α_1 and α_2. Performing analogous calculations as in the previous case and introducing an independent parameter r instead of u, we obtain the following parametric representation of the boundary:

$$\alpha_1^m = \left(1 + R_1(r)\right)^2 \left(1 + r^\gamma\right) \Big/ \left(R_1(r)\gamma\beta r^{\gamma-1}\right),$$

$$\alpha_2^m = \left(R_1(r)\right)^{1/\beta} \left(1 + r^\gamma\right), \tag{B.3}$$

where r is the parameter and

$$R_1(r) = -\frac{(\gamma-1) - r^\gamma(1+\beta\gamma)}{(\gamma-1) - r^\gamma(1-\beta\gamma)}. \tag{B.4}$$

Appendix C. The approximation for the Andronov–Hopf bifurcation. The Andronov–Hopf bifurcation curve for vanishing ε is approximated by the curve in the parameter space that corresponds to the intersection of the nullcline of slow motion with the manifold of slow motion in an extremum of the latter:

$$-F(u) + \alpha_3 h(\alpha_4 g(u)) = 0, \quad F'(u) = 0.$$

Let us solve this condition with respect to the parameters α_1 and α_2. This case is very similar to the condition of the boundary for the saddle-node bifurcation for the fast subsystem in the absence of the autoinducer (see Appendix A) because the only difference is the additive term $\alpha_3 h(\alpha_4 g(u))$. This term depends only on u and parameters α_3 and α_4, which gives us a possibility to apply the same steps as in the previous case, defining $R_3(u) = \alpha_3 h(\alpha_4 g(u))$. These calculations give the following curve in (α_1, α_2) parameter plane:

$$\alpha_1^H = \left(1 + R_2(r)\right) / \left(r - R_3(r)\right), \quad \alpha_2^H = \left(R_2(r)\right)^{1/\beta} \left(1 + r^\gamma\right), \tag{C.1}$$

where r is an independent parameter and

$$R_2(r) = \frac{\beta\gamma r^{\gamma-1}\left(r - R_3(r)\right)}{\left(\beta\gamma r^\gamma - r^\gamma - \beta\gamma r^{\gamma-1} R_3(r) - 1\right)} - 1,$$

$$R_3(r) = \alpha_3 \left(\frac{\alpha_4}{1+r^\gamma}\right)^\eta \Big/ \left(1 + \left(\frac{\alpha_4}{1+r^\gamma}\right)^\eta\right). \tag{C.2}$$

Acknowledgments. The authors thank James Collins, Tasso Kaper, and Horacio Rotsteine for useful discussions.

REFERENCES

[1] T. S. Gardner, C. R. Cantor, and J. J. Collins, *Construction of a genetic toggle switch in Escherichia coli*, Nature, 403 (2000), pp. 339–342.
[2] M. B. Elowitz and S. Leibler, *A synthetic oscillatory network of transcriptional regulators*, Nature, 403 (2000), pp. 335–338.
[3] C. C. Guet, M. B. Elowitz, W. Hsing, and S. Leibler, *Combinatorial synthesis of genetic networks*, Science, 296 (2002), pp. 1466–1470.
[4] Y. Yokobayashi, R. Weiss, and F. H. Arnold, *Directed evolution of a genetic circuit*, Proc. Natl. Acad. Sci. USA, 99 (2002), pp. 16587–16591.
[5] M. R. Atkinson, M. A. Savageau, J. T. Myers, and A. J. Ninfa, *Development of genetic circuitry exhibiting toggle switch or oscillatory behavior in Escherichia coli*, Cell. 113 (2003), pp. 597–607.
[6] W. Weber and M. Fussenegger, *Artificial mammalian gene regulation networks—novel approaches for gene therapy and bioengineering*, J. Biotechnol., 98 (2002) pp. 161–187.
[7] J. Hasty, D. McMillen, and J. J. Collins, *Engineered gene circuits*, Nature, 420 (2002), pp. 224–230.
[8] M. L. Simpson, G. S. Sayler, J. T. Fleming, and B. Applegate, *Whole-cell biocomputing*, Trends Biotechnol., 19 (2001), pp. 317–323.
[9] M. Kærn, W. Blake, and J. J. Collins, *The engineering of gene regulatory networks*, Ann. Rev. Biomed. Eng., 5 (2003), pp. 179–206.
[10] H. Kobayashi, M. Kærn, M. Araki, K. Chung, T. S. Gardner, C. R. Cantor, and J. J. Collins, *Programmable cells: Interfacing natural and engineered gene networks*, Proc. Natl. Acad. Sci. USA, 101 (2004), pp. 8414–8419.
[11] R. Weiss and T. Knight, *Engineered communications for microbial robotics*, in DNA6: Sixth International Meeting on DNA Based Computers, DNA 2000, Boston, MA, Springer-Verlag, New York, 2000, pp. 1–16.
[12] L. You, R. S. Cox 3rd, R. Weiss, and F. H. Arnold, *Programmed population control by cell-cell communication and regulated killing*, Nature, 428 (2004), pp. 868–871.
[13] S. Basu, R. Mehreja, S. Thiberge, M. T. Chen, and R. Weiss, *Spatiotemporal control of gene expression with pulse-generating networks*, Proc. Natl. Acad. Sci. USA, 101 (2004), pp. 6355–6360.
[14] C. Fuqua and P. E. Greenberg, *Listening in on bacteria: Acyl-homoserine lactone signaling*, Nat. Rev. Mol. Cell Biol., 3 (2002), pp. 685–695.
[15] M. K. Winson, S. Swift, L. Fish, J. P. Throup, F. Jorgensen, S. R. Chhabra, B. W. Bycroft, P. Williams, and G. S. Stewart, *Construction and analysis of luxCDABE-based plasmid sensors for investigating N-acyl homoserine lactone-mediated quorum sensing*, FEMS Microbiol. Lett., 163 (1998), pp. 185–192.
[16] M. Burmolle, L. H. Hansen, G. Oregaard, and S. J. Sorensen, *Presence of N-acyl homoserine lactones in soil detected by a whole-cell biosensor and flow cytometry*, Microb. Ecol., 45 (2003), pp. 226–236.
[17] J. B. Andersen, A. Heydorn, M. Hentzer, L. Eberl, O. Geisenberger, B. B. Christensen, S. Molin, and M. Givskov, *Gfp-based N-acyl homoserine-lactone sensor systems for detection of bacterial communication*, Appl. Environ. Microbiol., 67 (2001), pp. 575–585.
[18] D. McMillen, N. Kopell, J. Hasty, and J. J. Collins, *Synchronizing genetic relaxation oscillators by intercell signaling*, Proc. Natl. Acad. Sci. USA, 99 (2002), pp. 679–684.
[19] E. M. Ozbudak, M. Thattai, I. Kurtser, A. D. Grossman, and A. van Oudenaarden, *Regulation of noise in the expression of a single gene*, Nat. Gene., 31 (2002), pp. 69–73.
[20] J. Paulsson and M. Ehrenberg, *Noise in a minimal regulatory network: Plasmid copy number control*, Q. Rev. Biophys., 34 (2001), pp. 1–59.
[21] P. S. Swain, M. B. Elowitz, and E. D. Siggia, *Intrinsic and extrinsic contributions to stochasticity in gene expression*, Proc. Natl. Acad. Sci. USA, 99 (2002), pp. 12795–12800.
[22] T. F. Weiss,*Cellular Biophysics*, Vol. 1, MIT Press, Cambridge, MA, 1986.
[23] L. Perko, *Differential Equations and Dynamical Systems*, Springer-Verlag, New York, 1991.
[24] G. S. Medvedev and N. Kopell, *Synchronization and transient dynamics in the chains of electrically coupled FitzHugh–Nagumo oscillators*, SIAM J. Appl. Math., 61 (2001), pp. 1762–1801.

[25] A. Pikovsky, O. Popovuch, and Yu. Maistrenko, *Resolving clusters in chaotic ensembles of globally coupled identical oscillators*, Phys. Rev. Lett., 87 (2001), pp. 044102-1–044102-4.

[26] V. N. Belykh, I. V. Belykh, and M. Hasler, *Hierarchy and stability of partially synchronous oscillations of diffusively coupled dynamical systems*, Phys. Rev. E (3), (2000), pp. 6332–6345.

[27] N. Kopell, L. F. Abbott, and C. Soto-Trevino, *On the behaviour of a neural oscillator electrically coupled to a bistable element*, Phys. D, 121 (1998), pp. 367–395.

[28] K. A. Egland and E. P. Greenberg, *Conversion of the vibrio fischeri transcriptional activator,* LuxR, *to a repressor*, J. Bacteriol., 182 (2000), pp. 805–811.